Journal of The
Electrochemical Society

Review—Modelling Catalyst Layer Performance in Device-Scale Polymer Electrolyte Membrane Fuel Cell Simulation

To cite this article: Edmund J. F. Dickinson and Oliver Rodríguez 2024 *J. Electrochem. Soc.* **171** 064507

Journal of The Electrochemical Society, 2024 **171** 064507

Review—Modelling Catalyst Layer Performance in Device-Scale Polymer Electrolyte Membrane Fuel Cell Simulation

Edmund J. F. Dickinson[a] **and Oliver Rodríguez**[z]

National Physical Laboratory, Teddington TW11 0LW, United Kingdom

Theoretical models used to describe the catalyst layers (CLs) in polymer electrolyte membrane fuel cells (PEMFCs) are reviewed, with a focus on continuum treatments as incorporated in device-scale models used to predict and optimise PEMFC operating performance. Consideration is given to the mathematical relationships between CL design properties (Pt/C mass ratio, catalyst loading, ionomer loading), and physical properties. Relevant physical models are summarised, considering couplings between the CL and the phenomena of charge transfer, reactant mass transfer, hydrogen oxidation, and oxygen reduction electrode kinetics, heat transfer, and water balance. The relevance of thin film methods (through-thickness homogenisation) is compared to those resolving the macroscopic depth of the CL. Specific continuum homogenisations of microstructural models incorporating CL transport limitations in a continuum treatment, such as the agglomerate model, are discussed.

 [DOI: 10.1149/1945-7111/ad5408]

Manuscript submitted October 12, 2023; revised manuscript received February 15, 2024. Published June 27, 2024.

Table of Symbols

Symbol	Unit	Definition
a	1	Percolation theory probability distribution coefficient
a_{agg}	m^{-1}	Interfacial surface area at surface of agglomerate particles
a_{CL}	m^{-1}	Electroactive area per unit volume of CL material
$a_{Pt,sp}$	$m^2\ kg^{-1}$	Specific electroactive area (per unit mass of loaded Pt)
a_w	1	Activity, water in ionomer phase
b	1	Percolation theory probability distribution coefficient
C_p	$J\ K^{-1}\ kg^{-1}$	Specific heat capacity (mass-averaged)
c_i	$mol\ m^{-3}$	Concentration, species i
$c_{i,k}$	$mol\ m^{-3}$	Concentration, species i in phase k
$c_{i,ref}$	$mol\ m^{-3}$	Reference concentration, species i
$c_{eq,i,k}$	$mol\ m^{-3}$	Equilibrium concentration, species i in phase k
$D_{i,k}$	$m^2\ s^{-1}$	Diffusion coefficient, species i in phase k
D_{cap}	$m^2\ s^{-1}$	Capillary diffusion coefficient (effective), two-fluid model
$D_{eff,i,k}$	$m^2\ s^{-1}$	Effective diffusion coefficient, species i in phase k
$D_{K,i}$	$m^2\ s^{-1}$	Knudsen diffusion coefficient, species i
$\hat{D}_{ij}$	$m^2\ s^{-1}$	Maxwell-Stefan diffusion coefficient, species i,j
$\bar{D}_{eff,ij}$	$m^2\ s^{-1}$	Effective binary diffusion coefficient, species i,j
$\hat{D}_{eff,ij}$	$m^2\ s^{-1}$	Effective Maxwell-Stefan diffusion coefficient, species i,j
d_{CL}	m	Thickness, catalyst layer
d_{film}	m	Ionomer film thickness, agglomerate model
d_w	m	Water film thickness, ionomer model
d_{Pt}	m	Pt particle diameter
E_{OCV}	V	Open-circuit voltage
$E_{eq,m}$	V	Open-circuit potential, electrode m
F	$C\ mol^{-1}$	Faraday constant
f_{iono}	1	Proportion of ionomer in Pt/C-ionomer
f_{Pt}	1	Proportion of Pt in Pt/C
f_s	1	Shear interaction coefficient, two-fluid model
h_s	m	Characteristic curvature length scale
ΔH_{vap}	$J\ mol^{-1}$	Enthalpy change of vaporisation, water
$\mathbf{I}$	1	Unit tensor
$\mathbf{i}_l$	$A\ m^{-2}$	Macroscopic current density, electrolyte phase
$\mathbf{i}_s$	$A\ m^{-2}$	Macroscopic effective current density, electrode phase (per unit cross-section of composite material)
i_{act}	$A\ m^{-2}$	Current density from concentration-independent part of electrode kinetic expression
$i_{geom,CL}$	$A\ m^{-2}$	Current density (per unit electrode area)
i_{loc}	$A\ m^{-2}$	Interfacial current density (with respect to electroactive area)
$i_{ref,m}$	$A\ m^{-2}$	Apparent exchange current density, electrode m
$i_{ref,0}$	$A\ m^{-2}$	Apparent exchange current density, dry conditions
$i_{ref,v,m}$	$A\ m^{-3}$	Apparent exchange current density per unit composite volume of CL, electrode m
$i_{v,loc}$	$A\ m^{-3}$	Interfacial current per unit volume of CL material
$\mathbf{J}_i$	$kg\ m^{-2}\ s^{-1}$	Mass flux, species i
$K_{H,i,k}$	$Pa\ m^3\ mol^{-1}$	Henry's law coefficient, dissolution of species i in phase k
$k_{ads,Pt}$	$m\ s^{-1}$	Adsorption rate constant, O_2 on Pt
k_{agg}	s^{-1}	Irreversible first-order rate constant, agglomerate interior
k_c	s^{-1}	Rate constant, condensation of water
k_{eff}	$W\ m^{-1}\ K^{-1}$	Effective thermal conductivity (per unit cross-section of composite material)

[a]Present address: Energy Ltd, Railway Arch 8, Chancel Street, London SE1 0UR, United Kingdom.
[z]E-mail: oliver.rodriguez.martinez@npl.co.uk

$k_{\mathrm{sol},i,k}$	m s^{-1}	Rate constant, dissolution of species i in phase k
k_{v}	s^{-1} Pa^{-1}	Rate constant, evaporation of water
$k_{\mathrm{v,areal}}$	kg m^{-2} s^{-1} Pa^{-1}	Rate constant per unit area, evaporation of water
L_{vap}	J kg^{-1}	Latent heat of vaporisation
M	1	Exponent, percolation theory
M_i	kg mol^{-1}	Molar mass, species i
m_D	1	Exponent, tortuosity correction from liquid water saturation
m_{Pt}	kg m^{-2}	Mass loading of Pt per unit electrode area
$\mathbf{N}_{i,k}$	mol m^{-2} s^{-1}	Molar flux, species i in phase k
$\mathbf{N}_{\mathrm{diff},i}$	mol m^{-2} s^{-1}	Molar diffusive flux, species i
$N_{\mathrm{sol},i}$	mol m^{-2} s^{-1}	Interfacial dissolution rate, species i
$\mathbf{n}$	1	Normal vector (outward from specified material)
n_m	1	Number of electrons transferred, reaction m
n_{CL}	1	Exponent, loss of interfacial area from saturation
n_D	1	Exponent, tortuosity correction from dry porosity
$n_{\mathrm{vol,agg}}$	m^{-3}	Number density, agglomerates (per dry material volume)
$n_{\mathrm{vol,Pt}}$	m^{-3}	Number density, Pt particles
P	1	Probability density function (by volume)
p	Pa	Pressure
p_i	Pa	Partial pressure in gas phase, species i
p_{A}	Pa	Absolute pressure, gas phase
p_{cap}	Pa	Capillary pressure
p_{ref}	Pa	Reference pressure
p_{vap}	Pa	Vapour pressure, water
$p_{\mathrm{vap},0}$	Pa	Reference vapour pressure, water
$p_{\mathrm{vap,app}}$	Pa	Apparent vapour pressure, water
Q_T	W m^{-3}	Volumetric heat source
$Q_{T,\mathrm{far},m}$	W m^{-3}	Volumetric heat source, activation losses, reaction m
$Q_{T,IR}$	W m^{-3}	Volumetric heat source, resistive losses
$Q_{T,\mathrm{vap}}$	W m^{-3}	Volumetric heat source, evaporation-condensation
$\mathbf{q}$	W m^{-2}	Heat flux (per unit cross-section of composite material)
R	J K^{-1} mol^{-1}	Gas constant
$R_{\mathrm{diff},i}$	mol m^{-3} s^{-1}	Diffusion-limited reaction source of species i per unit volume of CL material
$R_{\mathrm{far},i}$	mol m^{-3} s^{-1}	Faradaic reaction source of species i per unit volume of CL material
$R_{\mathrm{m},i}$	kg m^{-3} s^{-1}	Net mass source from reactions, species i
$R_{\mathrm{m,vap}}$	kg m^{-3} s^{-1}	Net mass source of vaporisation
$R_{\mathrm{w},j\to k}$	mol m^{-3} s^{-1}	Effective molar reaction rate, evaporation-condensation of water from phase j to phase k
r_i	m	Pore radius of peak i in porosity distribution (Eikerling model)
r_{agg}	m	Agglomerate particle radius
r_{crit}	m	Critical capillary radius
r_{p}	m	Gas pore radius
r_{Pt}	m	Radius of Pt particle
r_{pp}	m	Primary pore radius
r_{ps}	m	Secondary pore radius
s_i	m	Width of peak i in porosity distribution (Eikerling model)
s_{l}	1	Saturation, liquid water (as volume fraction of pore volume)
$s_{\mathrm{l,p}}$	1	Saturation, liquid water in primary pores
T	K	Temperature
t_{per}	1	Exponent, percolation theory
$\mathbf{u}$	m s^{-1}	Velocity
$\mathbf{u}_k$	m s^{-1}	Effective (Darcy) velocity, phase k
V_k	m^3	Volume of phase/component k
$\nu_{i,m}$	1	Stoichiometric coefficient, species i in reaction m
x_i	1	Mole fraction, species i
α_m	1	Transfer coefficient, reaction kinetics at electrode m
β_{Pt}	1	Thiele modulus, individual Pt particle
β_{T}	1	Thiele modulus, agglomerate model
$\beta_{\mathrm{T,Pt}}$	1	Thiele modulus, agglomerate model with discrete Pt particle effects
γ	N m^{-1}	Surface tension
γ_{inact}	1	Proportion of blocked electroactive surface on agglomerate particles
ε_k	1	Volume fraction of phase/component k
$\varepsilon_{\mathrm{crit}}$	1	Critical volume fraction, percolation theory
η_m	V	Overpotential, electrode m
$\theta_{i,\mathrm{soln,iono}}$	K	Activation temperature, dissolution of species i in ionomer
θ_{c}	rad	Contact angle
κ_k	m^2	Permeability, phase k
κ_{eff}	S m^{-1}	Effective electrolyte conductivity (per unit-cross section of composite material)
κ_{iono}	S m^{-1}	Electrolyte conductivity, bulk ionomer (membrane material)
λ	1	Water content, ionomer phase, as ratio to concentration of sulfonic acid groups
λ_{sat}	1	Water content at equilibrium with pure water, ionomer phase (ratio of concentration of sorbed water to concentration of sulfonic acid groups)
μ_k	Pa s	Viscosity, phase k
μ_{w}	Pa s	Viscosity, liquid water
ξ	1	Agglomerate effectiveness factor
ρ	kg m^{-3}	Density (volume-averaged)
ρ_i	kg m^{-3}	Dry density, material i
ρ_k	kg m^{-3}	Density, phase k
$\sigma_{s,\mathrm{eff}}$	S m^{-1}	Effective electrode conductivity (per unit cross-section of composite material)
τ_k	1	Tortuosity, phase/component k
ϕ_l	V	Electrolyte potential
φ_{mt}	Pa s m^3 mol^{-1}	Generalised mass transfer characteristic, agglomerate structure
ϕ_s	V	Electric potential, electron-conductive phase
χ_{ps}	1	Relative volume contribution of secondary pores (Eikerling model)
χ_{res}	1	Residual electroactive area proportion (percolation theory)
ω_i	1	Mass fraction, species i

In a polymer electrolyte membrane fuel cell (PEMFC), both electrode reactions—the hydrogen oxidation reaction (HOR) at the anode and the oxygen reduction reaction (ORR) at the cathode—take place in a so-called "catalyst layer" (CL). The CLs are porous composites, specifically comprising a mixture of electrocatalyst (e.g. Pt) on a conductive support (e.g. carbon black) and polymer electrolyte (ionomer, e.g. perfluorosulphonic acid (PFSA)) with other additives sometimes present. As the only site of contact between electronic and ionic conductors in the fuel cell, the CL may also be referred to simply as the "electrode." The CL is conventionally adhered to the bulk membrane as a catalyst-coated membrane (CCM) and in industrial preparation may be provided as a membrane-electrode assembly (MEA), in which an electrolyte-free but electrically conductive gas diffusion layer (GDL) is bonded to the CL on each face of the membrane as a single assembly. Often, a microporous layer (MPL) with smaller average pore size is introduced between the GDL and CL.

In the present state-of-the-art for fuel cell modelling, there remains significant uncertainty concerning the most appropriate description of the CLs, despite thirty years of research in the field. The historical focus in model development has generally been on the cathode catalyst layer (CCL), due to the larger activation overpotential and greater transport losses associated with the ORR as compared to the comparatively brisk HOR. An accurate CL model is essential for performance-oriented device-scale modelling, as through-plane and nanoscale mass transport in the CL can be significant to the macroscopic current density response under PEMFC loads and environmental conditions of practical interest.[1,2] Likewise, phenomena in the CL impact directly on proton and liquid water balance across the cell, and on the contribution of electrochemical heat sources to local temperature non-uniformity.

Scope and Limitations

Previously reported relevant works focus on compiling the models on a descriptive level;[3–5] others focus on specific areas of the PEMFC such as CL degradation[6] or mass transport.[7,8] Instead, our review gives an account of continuum theories and their corresponding equations developed to describe the performance, mass, and charge transfer of PEMFC catalyst layers with traditional chemistry (platinum on carbon with PFSA ionomer), within device-scale models. Our aim is to offer a digest of theoretical methods, without listing exhaustively the many distinct simulations reported in the literature. In doing so, we also aim to highlight where there is a lack of agreement between academic practitioners, and where assumptions or parameterisation sources deviate from contemporary materials. Most of the specific models discussed in our review relate to the cathode CL. Since kinetics and catalyst utilisation are much more demanding to optimise at the cathode, which is usually the site of both the most significant activation and transport losses, very few analyses have evaluated the anode catalyst layer in detail. Some exceptions have been reported.[9–11]

Other works, such as that of Sui et al.,[5] have discussed microstructure-resolved and nanoscale theory of the CL, while De Lile and Zhou[12] have reviewed relevant work in atomistic simulation. These works, where mesoscopic, microscopic, and hierarchical methods are used, are outside the scope of this review, in which we focus on the continuum description of the CL at device-scale. Here, we make the clarification that by "device-scale" we mean "single-cell scale" as opposed to "microscopic scale," where macroscopic phenomena such as transport on flow channels are ignored. Some reports of simulations at the "stack-scale" level can be found for design optimization in mass transport and heat conduction, as well as catalyst durability in real-world conditions.[13–15] Generally, single cell scale simulations assume in-plane homogeneity, reducing the problem to the 1-dimensional (1D) space;[16] however, for stack-scale devices, this assumption may not be valid, and 3-dimensional (3D) problems are the norm.[17] To alleviate the computational cost of solving 3D simulations, some works have used a mix of these, where electrochemical reactions are simulated in 1D and the transport through channels in 3D; see for example Tsukamoto et al.[18]

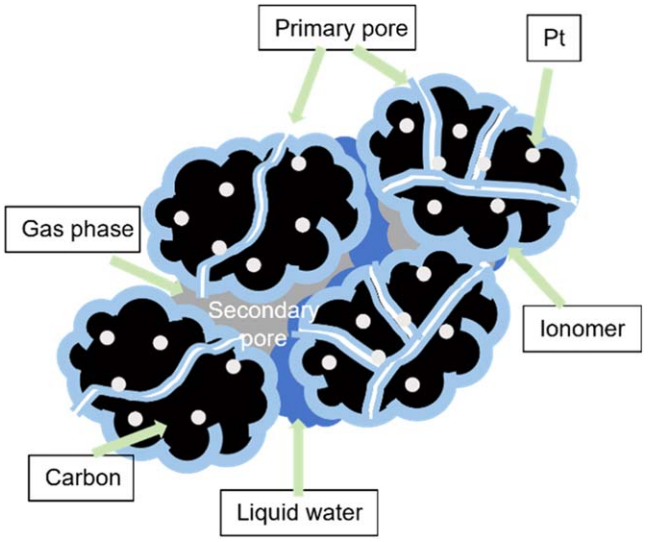

Figure 1. General structure of the catalyst layer. Catalyst (Pt nanoparticles of 2 nm to 10 nm in diameter) is embedded in support (carbon particles of 20 nm to 70 nm in diameter) that forms agglomerates with ionomer (100 nm to 400 nm in diameter). Primary pores exist within agglomerates while secondary pores exist between agglomerates. Pore space may contain gas phase and/or liquid water.

This review follows from other practical, device simulation-oriented works published previously by our group on PEMFC electrode kinetics[19] and the polymer electrolyte membrane;[20] we have also previously addressed two-phase catalyst layer models (i.e. those explicitly treating liquid water) in a report[21] that has been extensively revised to provide the content of the section on two-phase models of the catalyst layer.

Structure and Composition of the Catalyst Layer

The conventional CL is a composite of electrocatalyst, conductive support and ionomer. Its thickness, d_{CL}, is $\leqslant 20\ \mu$m. Pore space in the CL can be filled with liquid water and/or reactant/product gas, with the prominent gaseous components being H_2 and H_2O on the anode (fuel) side, and O_2, N_2 and H_2O on the cathode (air) side. The CL exhibits complex morphology and pore-size distribution, demanding intricacy from any suitable electrochemical and transport model. In particular, the electrocatalyst and its support form microporous agglomerates with the ionomer that give the CL a secondary morphological structure (Fig. 1).

Representative properties of a modern CL were reported by Kneer and Wagner in the context of a catalyst degradation model.[22] Their MEA consisted of a CL with a Pt nanoparticle loading of 0.25 mg cm^{-2} on the cathode and 0.10 mg cm^{-2} on the anode, embedded on a high surface area carbon support. The assembly was completed with a membrane layer (15 μm thickness) and two Sigracet SGL 25BIH gas diffusion layers. From scanning electron microscopy (SEM) and transmission electron microscopy (TEM) the average Pt particle size was determined to be 5.3 nm with a cathode thickness of 9.4 μm.

The complex morphology of the CL discourages the formulation of device-scale models that represent the microstructure literally; instead, by local volume-averaging, many continuum constitutive properties of the catalyst layer can be specified, along with their conservation relations, without specific reference to the microstructural morphology. A morphological model can then be incorporated subsequently to express the kinetics of source terms and the magnitudes of fluxes for non-equilibrium properties, as a function of average local composition and state.

Table I. Typical phases present in a PEMFC (columns), with an indication of corresponding regions where these phases are present, and relevant transport processes (solid circles) and source/sink couplings between phases (open circles). Non-isothermal models may add heat transport, sources and sinks to all phases and regions.

	Ionomer	Liquid water phase	Gas phase	Electrical conductors
Regions	Membrane, CL	CL, GDL	CL, GDL	CL, GDL
Processes				
Proton current density	●			
Electron current density				●
Bulk mass and momentum conservation		●	●	
Transport of gas-phase species: H_2, O_2, N_2, H_2O			●	
Transport of dissolved gases: H_2, O_2, N_2	●	●		
Transport of H_2O(l)	●	●		
Dissolution reactions	○	○	○	
Condensation-evaporation		○	○	
Faradaic mass source	○	○	○	
Faradaic current source	○			○

Common to all homogenised descriptions of the CL is the representation of its average composition. Volume fractions ε_k of phase k are defined in terms of the corresponding volumes of all phases q, V_q, (m^3) present in the CL:

$$\varepsilon_k = \frac{V_k}{\sum_q V_q} \quad [1]$$

The following specific phases have associated volume fractions ε:

ε_{gas}—gas (multi-component mixture)
ε_w—liquid water
ε_{iono}—ionomer (i.e. polymer electrolyte material, e.g. Nafion)
ε_C—conductive catalyst support (i.e. carbon)
ε_{Pt}—electrocatalyst (i.e. Pt)

These volume fractions can also be grouped as follows:

ε_{agg}—volume occupied by a microporous agglomerate of carbon black particles and Pt, including primary pores between/within the constituent particles of the agglomerate but not including ionomer film on the agglomerate surfaces

ε_{pore}—volume occupied by secondary pores between agglomerate structures, connected to the GDL (may be partially or fully saturated with liquid water)

ε_{CL}—combined porosity due to primary and secondary pores

The contents of the CL are usually defined in terms of a chosen Pt mass loading per unit electrode area (m_{Pt}, kg m^{-2}), together with the Pt mass fraction in Pt/C (f_{Pt}) and the ratio of ionomer loading to total ionomer and catalyst (Pt/C) loading (f_{mem}).[9,23] Hence if ρ_i denotes the dry density of material i, including primary pores:

$$\varepsilon_{Pt} = \frac{m_{Pt}}{\rho_{Pt}} \frac{1}{d_{CL}} \quad [2]$$

$$\varepsilon_C = \varepsilon_{Pt} \left(\frac{1 - f_{Pt}}{f_{Pt}} \right) \frac{\rho_{Pt}}{\rho_C} \quad [3]$$

$$\varepsilon_{iono} = \frac{1}{\rho_{iono} d_{CL}} \left(\frac{f_{iono}}{1 - f_{iono}} \right) \frac{m_{Pt}}{f_{Pt}} \quad [4]$$

If all Pt/C is assumed to form agglomerates, and all ionomer is assumed to be associated with the agglomerates as a film, the above formulas are combined to give aggregated volume fractions for the specific agglomerate volume fraction as[b,23]:

$$\varepsilon_{agg} = \frac{m_{Pt}}{d_{CL}} \left(\frac{1}{\rho_{Pt}} + \frac{1 - f_{Pt}}{f_{Pt} \rho_C} \right) \quad [5]$$

$$1 - \varepsilon_{pore} = \varepsilon_{agg} + \varepsilon_{iono} = \frac{m_{Pt}}{d_{CL}} \left(\frac{1}{\rho_{Pt}} + \frac{1 - f_{Pt}}{f_{Pt} \rho_C} + \frac{f_{iono}}{f_{Pt}} \frac{1}{(1 - f_{iono}) \rho_{iono}} \right) \quad [6]$$

The volumetric current density $i_{v,loc}$ (A m^{-3}) can be expressed in terms of volumetric electroactive surface area a_{CL} (m^{-1}, i.e. m^2 per m^3 of total composite volume), and an effective current density i_{loc} (A m^{-2}):

$$i_{v,loc} = a_{CL} i_{loc} \quad [7]$$

We note that a_{CL} is sometimes called "specific (electroactive) surface area"; however, the term "specific" is by preference used only for quantities measured per unit mass. A typical value is $a_{CL} \approx 10^7$ m^{-1},[24] although the concept of an electrode–electrolyte contact area within the intricate morphology of the CL is effectively "in the eye of the beholder," since suitable parameterisation of specific current with respect to microscopic areal current density can make any definition compatible with a measured performance. The electroactive surface area per unit volume can be expressed in terms of the corresponding specific interfacial area per unit mass Pt, $a_{Pt,sp}$ (m^2 kg^{-1}):[25]

$$a_{CL} = \frac{m_{Pt} a_{Pt,sp}}{d_{CL}} \quad [8]$$

Typical values of $a_{Pt,sp}$ were tabulated in 1999 for industrially produced E-TEK catalyst (Pt on Vulcan carbon black, now sold by De Nora S.p.A, Milan, Italy).[9] A cubic fit to these data was derived[26] and used in some subsequent works.[27,28]

$$a_{Pt,sp}/m^2\ g^{-1} = 159.5 - 201.53 f_{Pt} - 158.57 f_{Pt}^2 + 227.79 f_{Pt}^3 \quad [9]$$

Given that the original data represent industrial standards from more than 20 years ago, the relevance of Eq. 9 to contemporary materials should be carefully appraised before use.

Transport, Sources, and Sinks

Volume-averaged conservation laws.—The conventional approach to continuum modelling of PEMFCs is to express differential equations governing fluxes, sources and sinks of transported quantities, which are treated as continuous by means of homogenisation of porous media. The relevant fluxes are ionic and electronic current densities; material fluxes of H_2, O_2, N_2, and

[b]The reader is alerted that Eq. 5 contains a sign error as stated in the full PEMFC model summary by Baschuk and Li, 2009 [J. J. Baschuk and X. Li, *Applied Energy*, **86**, 181 (2009)].

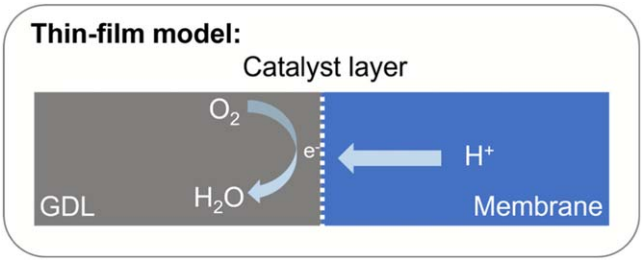

Figure 2. Schematic of the thin-film model. The catalyst layer is treated as a boundary between the gas diffusion layer and the membrane.

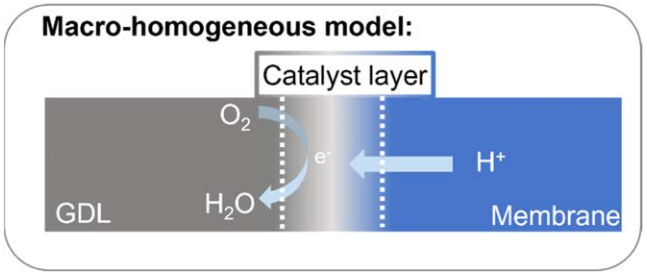

Figure 3. Schematic of the macro-homogeneous model. The catalyst layer has a defined thickness; transport, source and sink of species can occur concomitantly within its bulk.

H_2O in the gas phase; material flux of protons in ionomer; and material flux of liquid water; see Table I for a more comprehensive list. For some applications, heat flux and material fluxes of dissolved components in the ionomer phase may be considered. Since the adjoining GDL/MPL is insulating to ionic current, while the adjoining bulk membrane is insulating to electronic current, the CL is necessarily the site of all transfer between electronic and ionic current density, principally by means of faradaic reactions.

Thin-film model concept.—The thin-film model considers the catalyst layer as an infinitesimal boundary between the GDL and membrane (see Fig. 2). In this case, the following conservation relation applies:

$$-\mathbf{i}_{s,\mathrm{GDL}}\cdot\mathbf{n}_{\mathrm{GDL}} = \mathbf{i}_{l,\mathrm{mem}}\cdot\mathbf{n}_{\mathrm{mem}} = i_{\mathrm{geom,CL}} \quad [10]$$

In a thin film treatment, the variation of CL properties through the CL thickness is not explicitly included in the model. Thus, the CL model must express $i_{\mathrm{geom,CL}}$ as a function of its homogenised properties. The particular formulation of the expression $i_{\mathrm{geom,CL}}$ allows complexity to the influence of the CL on charge and mass transfer at the full-cell level. The significant limitation of thin film models is the absence of resolution between the GDL- and membrane-facing regions of the CL. By extension, fluxes of other properties can be expressed as discontinuous between the GDL/MPL and CL. That is, the CL is described as an infinitesimal source/sink of H^+, gas-phase reactants and products, liquid water, etc. Such a treatment can in principle account for transport losses in the catalyst layer only by means of a suitable functional dependence of the source/sink terms upon the dependent variables; however, it is more common to apply the thin-film approach when transport losses are ignored overall, such that the model applies only to the kinetically-controlled and ohmic regimes.[3,29–31]

Macro-homogeneous model concept.—The assumption that the CL does not need to be resolved spatially[32] rests generally on the recognition that it is sufficiently thin for through-layer pressure differences to be negligible, even in the liquid phase.[33] Where a volumetric resolution is attempted, difficulty arises because the CL is challenging to access experimentally due to its small dimensional extent. Nonetheless, the 1D resolution of the CL thickness, considering variation in composition and state between the GDL–CL and membrane–CL interfaces, has been the most popular approach historically. Termed the "macro-homogeneous" model (Fig. 3), this approach began with the works by Bernardi et al. and Springer et al.[34,35]

In macro-homogeneous models, transport equations are extended for the relevant phases from the adjacent GDL and membrane regions, taking into account the different volume fractions of each CL component.[34–38] Then, the governing variables and superficial fluxes of each conserved quantity can be made continuous at the GDL-CL boundary (for solid, gas and liquid water phases) and at the PEM-CL boundary (for ionomer phase). Volumetric source/sink terms are defined for a specific location within the homogenised CL, as opposed to the total source/sink terms for the entire CL as in Eq. 10.

Transport in Macro-homogeneous Models

Charge transfer.—Considering the effective (composite volume-averaged) current density in the electron-conducting solid phase ($\mathbf{i}_s$) as being continuous with the GDL, and the electrolyte current density in the ionomer phase ($\mathbf{i}_l$) as being continuous with the membrane, the volumetric current conservation equations are:

$$\nabla\cdot\mathbf{i}_s = -i_{v,\mathrm{loc}} \quad [11]$$

$$\nabla\cdot\mathbf{i}_l = +i_{v,\mathrm{loc}} \quad [12]$$

A common general approach to account for charge transfer is to use Ohm's law for both electrode and electrolyte current densities:[39]

$$\mathbf{i}_s = -\sigma_{s,\mathrm{eff}}\nabla\phi_s \quad [13]$$

$$\mathbf{i}_l = -\kappa_{\mathrm{eff}}\nabla\phi_l \quad [14]$$

where $\sigma_{s,\mathrm{eff}}$ and κ_{eff} are the effective conductivities of the electron-conducting and ion-conducting (electrolyte) phases respectively. Here, Eq. 14 is an extension of the equivalent expression used for the ionomer in the bulk membrane.

The current source $i_{v,\mathrm{loc}}$ used in Eqs. 11 and 12 is typically only due to electrocatalytic reactions, since even for transient studies, the timescales of interest are much longer than those relevant for capacitive currents.[40] Nonetheless, transient equations including a volume-averaged capacitive contribution have also been presented.[41]

The specification of $i_{v,\mathrm{loc}}$ depends on an electrode kinetic expression for the rate of the HOR or ORR as a function of local properties, which may in principle encompass the following: overpotential, water content, temperature, reactant concentrations, and compositional properties of the CL. Frequently chosen options include Tafel or Butler-Volmer equations—some critical discussion has been published by our group,[19] in which persistent errors in the formulation of the Butler-Volmer equation as used in PEMFC simulation were identified. For cases where PEMFC performance simulation is undertaken for standard operating conditions, simple treatments such as linear reversible kinetics for the HOR and irreversible Tafel kinetics for the ORR suffice.[37] For the case of non-standard operation, true mechanistic models—as distinct from the empirical Butler-Volmer equation—are preferred.

For any chemical species we can write, from Faraday's laws:

$$R_{\mathrm{far},i} = \sum_m -\nu_{im}\frac{i_{v,\mathrm{loc},m}}{n_m F} \quad [15]$$

where $R_{\mathrm{far},i}$ is the volume-averaged molar source due to the faradaic processes, and for reaction m, ν_{im} is the stoichiometric coefficient in the direction of reduction, and n_m is the total number of electrons transferred (standard values are given in Table II). This expression does not define the specific phase in which the reactants are present.

Table II. Standard stoichiometric coefficients for PEMFC reactions.

Quantity	m = HOR	m = ORR
n_m	2	4
$\nu_{H2,m}$	1	0
$\nu_{O2,m}$	0	−1
$\nu_{H2O,m}$	0	2
$\nu_{N2,m}$	0	0

Typical Pt/C agglomerate material may have effective electrical conductivity around 1000 S m^{-1}. Even for a very high current density of 5 A cm^{-2}, for d_{CL} = 20 μm this yields a steady-state potential drop in the solid-phase of only 1 mV. On this basis, it is commonly approximated that the potential of the electron-conducting phase is a constant,[42] thereby excluding Eq. 11 in favour of a specification of constant polarisation of the electron-conducting phase across the CL. Similarly, the transient response of the potential variables can be considered very fast compared to concentration changes, in a dynamic model.[41] Moreover, ohmic drop due to resistance in the electrolyte is often considered as less significant than reactant transport limitations.[9,42]

Measured values of electrolyte conductivity in the CL.—The effective electrolyte conductivity in the CL is lowered from its bulk value due to the tortuosity of the ionomer phase; some early authors suggested a linear dependence on ionomer volume fraction,[43,44] while another possible approach is to use the Bruggeman correlation:[45,46]

$$\sigma_{s,\text{eff}} = \sigma_s \varepsilon_{\text{agg}}^{3/2} \quad [16]$$

$$\kappa_{\text{eff}} = \kappa_{\text{iono}} \varepsilon_{\text{iono}}^{3/2} \quad [17]$$

where σ_s and κ_{iono} are bulk conductivities. The conditions used to derive the Bruggeman correlation require an isotropically random, macro-homogeneous dispersion of material—these conditions are not necessarily well satisfied for typical CL morphologies[46,47] nonetheless, the Bruggeman correlation has been applied widely.[9,23,27,28,48–54]

Eikerling et al. established a percolation theory to predict the effective electrolyte conductivity from its bulk value, considering the requirement for connectivity of electrolyte material to allow macroscopic conductivity.[36] This expression was simplified and re-used in later works as follows:[55,56]

$$\begin{aligned}\kappa_{\text{eff}} &= \kappa_{\text{iono}} \left(\frac{\varepsilon_{\text{iono}} - \varepsilon_{\text{crit}}}{1 - \varepsilon_{\text{crit}}} \right)^{t_{\text{per}}}, \quad \varepsilon_{\text{iono}} \geqslant \varepsilon_{\text{crit}} \\ &= 0, \quad \varepsilon_{\text{iono}} < \varepsilon_{\text{crit}}\end{aligned} \quad [18]$$

where $\varepsilon_{\text{crit}}$ is a limiting value to allow percolation to occur (suggested value of 0.1[56]), and $t_{\text{per}} \approx 2$ for general 3D pore networks.

In principle, a fuller charge transfer model for the ionomer phase could be used by analogy to the Weber-Newman model for the membrane;[20,57,58] however, the ionomer phase present in the catalyst layer is known to have properties that are quite distinct from the bulk phase[59] due to its nanostructural morphology, and so the use of the empirical Ohm's law (Eq. 14) allows a flexible and possibly more accurate approach. Due to the small thickness of the CL, the impact of a precisely chosen model is questionable—resistive losses due to finite electrolyte conductivity typically form a small contribution to the overall contribution of the CL, and a linear model is normally assumed to be sufficient.

Electrode kinetics.— *Thermodynamic reference point.*—The open-circuit voltage E_{OCV} of a cell is the voltage at which the total current is zero. Similarly, the open-circuit potential (equilibrium potential, $E_{\text{eq},m}$) of half-cell m is the voltage measured against a suitable reference electrode at which the electrode current is zero. From the Nernst equation, open-circuit potentials are necessarily concentration-dependent:

$$E_{\text{OCV}} = E_{\text{eq,ORR}} - E_{\text{eq,HOR}} \quad [19]$$

$$E_{\text{eq,HOR}} = E_{\text{eq,HOR,ref}} + f(c_{\text{H}_2}) \quad [20]$$

$$E_{\text{eq,ORR}} = E_{\text{eq,ORR,ref}} + f(c_{\text{O}_2}) \quad [21]$$

The equilibrium potential for the HOR is generally specified as $E_{\text{eq,HOR}} = 0$ V exactly. This definition is sound, in the sense that we may consider both ORR and HOR to be measured against a reference electrode exactly resembling the HOR under the local conditions of the anode. However, such an interpretation then creates ambiguity around the treatment of any concentration variations within the anode since the reference scale for equilibrium potentials is no longer matched to a global quantity.

The overpotential, η, represents the polarisation of a half-cell with respect to its open-circuit potential, and since the latter is concentration-dependent, so is the overpotential (a = anode; c = cathode):

$$\eta_a = \phi_s - \phi_l - E_{\text{eq,HOR}} \quad [22]$$

$$\eta_c = \phi_s - \phi_l - E_{\text{eq,ORR}} \quad [23]$$

For the oxygen reduction reaction, the measured open-circuit potential is lower than that expected from the thermodynamics of the O_2/H_2O couple (1.23 V) due to the presence of parasitic anodic processes at the electrode surface and nonzero H_2 crossover.[60] In practice, an empirically observed open-circuit potential, not a true equilibrium potential, must be specified to reproduce experimental observations.[60]

Simple models.—For models not exploring extreme regimes of transport limitation but instead focusing on standard operating conditions, the Wang-Um electrode kinetic model is the most appropriate.[19] This model assumes a linear current density-overpotential relation for the HOR and applies cathodic Tafel kinetics for the ORR. The simplest assumption for the concentration-dependences of the HOR and ORR is that they are linear in H_2 and O_2 partial pressure respectively. Hence, measured with respect to electroactive surface area:

$$i_{\text{loc,a}} = i_{\text{ref,a}} \frac{F}{RT} \eta_{\text{a}} \left(\frac{c_{\text{H}_2}}{c_{\text{H}_2,\text{ref}}} \right) \quad [24]$$

$$i_{\text{loc,c}} = -i_{\text{ref,c}} \exp\left(-\frac{\alpha_{\text{c}} F}{RT} \eta_{\text{c}} \right) \left(\frac{c_{\text{O}_2}}{c_{\text{O}_2,\text{ref}}} \right) \quad [25]$$

Typical apparent exchange current densities for the HOR have been reported in volumetric units as $i_{\text{ref,v,a}} = 5 \times 10^8$ A m^{-3},[37] and in flux units (with respect to electroactive area) as $i_{\text{ref,a}} = 10$ A m^{-2},[61,62] while typical apparent exchange current densities for the ORR are about $i_{\text{ref,v,c}} = 100$ A m^{-3};[37] however, intrinsic values in flux units up to 0.05 A m^{-2} have been reported.[62] Meanwhile, a common reference value for the Tafel slope of the ORR is $\alpha_{\text{c}} = 1$.[62,63]

Complex models.—For a consideration of conditions such as fuel starvation in which transport limitations arise at the anode, more complex electrode kinetic models may be considered. These models generally aim to capture the contribution of reaction intermediates.

For example, for the HOR, detailed mechanistic models are generally based on the Tafel-Heyrovský-Volmer mechanism, which has been discussed elsewhere.[64] Some modern models implement an

HOR kinetic model based on the rationalised Wang-Springer-Adzic "dual-pathway" kinetics in which the namesake pathways are the parallel Tafel-Volmer and Heyrovský-Volmer mechanisms for the overall two-electron oxidation.[65] Detailed mechanistic models for the ORR generally invoke either a blocking or participating role for PtOH and PtO surface species, the most developed of these is the "double trap" mechanism by J.X. Wang et al. and by Moore et al.[66–70]

Gas-phase mass transfer.—The gas-phase velocity in macro-homogeneous models can be described by extending the flow model used in the GDL, which generally uses the Navier–Stokes-Brinkman equations with Maxwell-Stefan equations for gas-phase species transport:[71]

$$\frac{\rho_g}{\varepsilon_{gas}^2}(\mathbf{u}\cdot\nabla)\mathbf{u} = -\nabla p + \nabla\cdot\left(\frac{1}{\varepsilon_{gas}}\left(\mu_g(\nabla\mathbf{u} + (\nabla\mathbf{u})^T) - \frac{2}{3}\mu_g(\nabla\cdot\mathbf{u})\mathbf{I}\right)\right) - \left(\frac{\mu_g}{\kappa_g} - \frac{\sum_i R_{m,i}}{\varepsilon_{gas}^2}\right)\mathbf{u} \quad [26]$$

$$\sum_i \omega_i = 1 \quad [27]$$

$$\boldsymbol{J}_i = -\rho_g \omega_i \sum_j \bar{D}_{\text{eff,ij}}\left(\nabla x_j + (x_j - \omega_j)\frac{\nabla p}{p_A}\right) \quad [28]$$

$$\hat{D}_{\text{eff},ij} = \frac{\varepsilon_{gas}}{\tau_{gas}}\hat{D}_{ij} \quad [29]$$

$$x_i = \frac{\frac{\omega_i}{M_i}}{\sum_j \frac{\omega_j}{M_j}} \quad [30]$$

$$\rho_g = \frac{p_A}{RT}\sum_i M_i x_i \quad [31]$$

$$p_A = p + p_{ref} \quad [32]$$

$\bar{D}_{\text{eff},ij}$ are defined from the Maxwell-Stefan diffusivities. $\hat{D}_{\text{eff},ij}$. as specified in standard textbooks.[71] These equations account for porous media effects by means of a specified permeability, porosity, and tortuosity of the connected gas-permeable regions of the CL. The gas-phase tortuosity is often given by a Bruggeman relation:

$$\tau_{gas} \approx \varepsilon_{gas}^{-1/2} \quad [33]$$

Given that transport of reactants in the gas phase is significantly faster than the corresponding permeability of H_2 and O_2 reactants dissolved in aqueous or ionomer phases, the degree of complexity implied by Eqs. 26 to 32 is often deemed excessive. It may be accurate to consider a uniform gas-phase partial pressure in the CL for each component species,[42,72] so that concentration gradients are present only in the dissolved phase.

Alternatively, gas-phase mass transport can be considered as purely diffusive, or through a combination of diffusion and convection driven by porous flow, with flow velocities derived using the above theory. According to a simple diffusion equation:

$$N_{\text{diff},i,gas} = -D_{\text{eff},i,gas}\,\nabla c_{i,gas} \quad [34]$$

At the short length scales of the microporous and mesoporous features of the CL, Knudsen diffusion becomes important—the use of a continuum diffusion coefficient underestimates measured diffusion coefficients.[73–75] The theoretical incorporation of concurrent continuum and Knudsen diffusion is given as follows:[74,76]

$$D_{\text{eff},i,gas} = \frac{\varepsilon_{gas}}{\tau_{gas}}\frac{1}{\frac{1}{D_{i,gas}} + \frac{1}{D_{K,i}}} \quad [35]$$

where $D_{i,gas}$ is a bulk Fick's law diffusion coefficient for component i in the gas phase, and $D_{K,i}$ is the Knudsen diffusion coefficient:

$$D_{K,i} = \frac{2r_p}{3}\sqrt{\frac{8RT}{\pi M_i}} \quad [36]$$

Heat transfer.—The general heat equation applied in PEMFC models is given as follows:

$$\rho C_p\frac{\partial T}{\partial t} + \nabla\cdot(\rho C_p T\mathbf{u} + \mathbf{q}) = Q_T \quad [37]$$

The general heat source applying throughout the fuel cell is the Joule heat source due to ohmic losses:

$$Q_{T,IR} = \frac{\mathbf{i}_l^2}{\kappa_{\text{eff}}} + \frac{\mathbf{i}_s^2}{\sigma_{s,\text{eff}}} \quad [38]$$

In the CL specifically, there is also a reaction heat source associated with the enthalpy of the HOR/ORR processes. For electrochemical reactions, this is expressed as follows:

$$Q_{T,\text{far},m} = i_{v,\text{loc},m}\left(\eta_m + T\frac{\partial E_{\text{eq},m}}{\partial T}\right) \quad [39]$$

For evaporation-condensation of water:

$$Q_{T,\text{vap}} = -L_{\text{vap}}R_{\text{vap}} \quad [40]$$

where R_{vap} is the volume-averaged vaporisation mass source (kg m^{-3} s^{-1}) and L_{vap} is the latent heat of vaporisation of water (specified in standard engineering references, $\approx$2260 kJ kg^{-1} at room temperature). The negative sign in Eq. 40 accounts for the fact that latent heats are conventionally defined with respect to the enthalpy of a chemical system, such that an endothermic process increases the enthalpy of the chemical system (positive L_{vap}) by removing heat from the surroundings.

The heat flux due to conduction is:

$$\mathbf{q} = -k_{\text{eff}}\nabla T \quad [41]$$

where, if all phases in the homogenised porous medium can be treated as at local thermal equilibrium (i.e. each phase is at the same temperature at the scale of microstructural averaging), the effective conductivity is an averaged transport property across all phases. There is wide disparity in the parameterisation of the effective conductivity depending on CL composition.[77–80]

The approximation of local thermal equilibrium may not be valid at the length scales of homogenisation for CLs—if it is not, a local thermal non-equilibrium (LTNE) model can be defined with distinct temperature fields for different phases within the same region of the homogenised phase.[81] Heat is exchanged between phases according to specified heat transfer coefficients for each pair of phases.

Dissolution and solution-phase mass transfer.—Transport phenomena in ionomer materials, such as electroosmotic drag and water condensation rate, have been reviewed previously.[20] Thin liquid water films (implying "flooding" of the CL) arise on ionomer-Pt/C agglomerates even at very low liquid water saturation.[82] Given that transport of reactants is orders of magnitude slower in condensed phases than in the gas-phase, blocking of the gas-phase transport

paths by flooding is a major contributor to transport limitations on PEMFC performance.

For reactant gases to undergo an electrochemical reaction, they must enter a solution phase—either in liquid water, or directly dissolved in the ionomer. H_2 and O_2 exhibit relatively low solubility and diffusivity in these phases: consequently, the apparent permeability of the gases in a condensed phase can be the principal transport limitation to catalyst layer performance, even when the thickness of water or ionomer films is no larger than 10 nm.[42]

Dissolution of reaction gases.—A common approach is to consider the dissolution of reactant gases in the condensed phases to be infinitely fast compared to the typical current densities of operation,[9,37,83–90] assuming a very high gas-ionomer contact area in the CL structure. In this case, at the interface with the gas phase, the concentration in phase k can be expressed using Henry's law:

$$c_{i,k} = c_{\mathrm{eq},i,k} = \frac{p_i}{K_{\mathrm{H},i,k}} \quad [42]$$

In principle, Henry's law coefficients for liquid water and ionomer are different,[86] but no distinct values are known to have been reported in the literature.

Reported values in ionomer are: $K_{\mathrm{H,O2,iono}} = 0.265$ atm m^3 mol^{-1} at $T = 50$ °C;[85] $K_{\mathrm{H,O2,iono}} = 0.2$ atm m^3 mol^{-1} at $T = 80$ °C.[37] These values are broadly compatible with the reported order-of-magnitude range of 10^{-15} to 10^{-14} mol m^{-1} s^{-1} Pa^{-1} for typical gas permeabilities in ionomer.[91] A generalised empirical expression depending on water content and temperature has been given by Xing et al.,[92] drawing on previous work considering dependence upon temperature[93] and ionomer water content λ:[94]

$$K_{\mathrm{H},\mathrm{O}_2,\mathrm{iono}} = K_{\mathrm{H},\mathrm{O}_2,\mathrm{iono},0} \exp\left(0.0302\lambda - \frac{\theta_{\mathrm{O}_2,\mathrm{soln},\mathrm{iono}}}{T}\right) \quad [43]$$

with $K_{\mathrm{H,O2,iono},0} = 1.515$ atm m^3 mol^{-1} and $\theta_{\mathrm{O2,soln,iono}} = 666$ K.

If dissolution is infinitely fast then Eq. 42 can be applied directly, but a finite rate of dissolution of reactant species can alternatively be defined.[94] The reactant dissolution rate $N_{\mathrm{sol},i}$ (mol m^{-2} s^{-1}) has been proposed as a linear function in concentration:[94,95]

$$N_{\mathrm{sol},i} = k_{\mathrm{sol},i,\mathrm{iono}}(c_{\mathrm{eq},i,\mathrm{iono}} - c_{i,\mathrm{iono}}) \quad [44]$$

As $k_{\mathrm{sol},i,\mathrm{iono}}$ tends to infinity in Eq. 44, the equality in Eq. 42 is recovered throughout the CL.

Suzuki et al. recommended that the finite rate of dissolution of reactant species must be included to introduce a resistive contribution to the performance of the CL.[94] This work attributed the oversizing of agglomerate particles in models, as compared to microscopy data, to the failure of previous models to include such a resistance.

The product $k_{\mathrm{sol,O2,iono}}c_{\mathrm{eq,O2,iono}}$ has been reported in the range 2×10^{-3} mol m^{-2} s^{-1} to 2×10^{-2} mol m^{-2} s^{-1} at 60% relative humidity.[94] For typical $D_{\mathrm{O2,iono}}$ values (see also later in this section), the dissolution resistance becomes rate-limiting for films of less than 100 nm thickness, as observed in measured CL morphology. Conversely, Moore et al. interpreted the data to give $k_{\mathrm{sol,O2,iono}} = 0.13$ m s^{-1}, and argued that this contributes negligibly to the overall resistance of the catalyst layer, whereas a hypothesised value of $k_{\mathrm{sol,O2,iono}} = 10^{-3}$ m s^{-1} would have an appreciable effect.[59] Liu et al. performed a similar analysis to that of Suzuki et al., but using a modified structure in which no Pt-ionomer interface exists.[96] They found negligible transport resistance in this case, and so argued that the overall thickness-independent transport resistance measured by Suzuki et al. should not be attributed to dissolution kinetics but rather to the altered accessibility of the Pt surface to the ORR due to adsorption or interaction of the ionomer.

In summary, the most suitable value of $k_{\mathrm{sol,O2,iono}}$ has not yet been firmly established. It may be that a low value of $k_{\mathrm{sol,O2,iono}}$ is simply one route to "add resistance" to the CL model and thereby bring prediction in line with observation, even though in reality the observed transport resistance arises from other phenomena.

Transport of reactant gases in the ionomer phase.—Some authors view oxygen transport in the CL as a combination of parallel diffusion in the gas phase and diffusion of dissolved O_2 through the ionomer.[97,98] In this context, Fick's law of diffusion is generally assumed for diffusion of O_2 in ionomer, where the apparent flux (per unit area of catalyst layer) is given in the macro-homogeneous direction as:

$$\mathbf{N}_{\mathrm{O}_2,\mathrm{iono}} = -D_{\mathrm{eff},\mathrm{O}_2,\mathrm{iono}} \nabla c_{\mathrm{O}_2,\mathrm{iono}} \quad [45]$$

The effective diffusivity depends on the volume fraction and tortuosity associated with the ionomer phase:

$$D_{\mathrm{eff},\mathrm{O}_2,\mathrm{iono}} = \frac{\varepsilon_{\mathrm{iono}}}{\tau_{\mathrm{iono}}} D_{\mathrm{O}_2,\mathrm{iono}} \quad [46]$$

A Bruggeman relation is often used[9,52,86,87,89,94,99–101] to define the tortuosity with respect to macro-homogeneous diffusion within the ionomer phase:

$$\tau_{\mathrm{iono}} = \varepsilon_{\mathrm{iono}}^{-1/2} \quad [47]$$

Over the full CL length scale, however, the ionomer-phase diffusivity is likely to have a negligible influence compared to gas-phase mass transport, since the diffusion in the dissolved phases is so slow that dissolution will tend to take place locally to the site of reaction. In the latter case, the influence of oxygen diffusion depends on the choice of microstructural model. Macroscopically across the whole CL, $D_{\mathrm{eff,O2,iono}}$ is almost always so small that it is approximately zero on the CL dimension, so its precise value has no significant effect. This may explain why there is no particular consistency in values of the diffusivity quoted by different authors;[9,23,85,94,102] to give one example, the following effective diffusion coefficient data (including H_2, uniquely) are given by Schwarz et al.:[103]

$$D_{\mathrm{H}_2,\mathrm{w}}/\mathrm{m}^2\ \mathrm{s}^{-1} = 3.34 \times 10^{-6} \exp\left(\frac{-1932\ \mathrm{K}}{T}\right)$$

$$D_{\mathrm{O}_2,\mathrm{w}}/\mathrm{m}^2\ \mathrm{s}^{-1} = 2.31 \times 10^{-6} \exp\left(\frac{-2055\ \mathrm{K}}{T}\right)$$

$$D_{\mathrm{H}_2,\mathrm{iono}}/\mathrm{m}^2\ \mathrm{s}^{-1} = 7.16 \times 10^{-8} \frac{\lambda}{\lambda_{\mathrm{sat}}} \exp\left(\frac{-1335\ \mathrm{K}}{T}\right)$$

$$D_{\mathrm{O}_2,\mathrm{iono}}/\mathrm{m}^2\ \mathrm{s}^{-1} = 2.67 \times 10^{-6} \frac{\lambda}{\lambda_{\mathrm{sat}}} \exp\left(\frac{-2870\ \mathrm{K}}{T}\right) \quad [48]$$

Values for O_2 diffusivity in liquid water close to $D_{\mathrm{O2,w}} = 5 \times 10^{-9}$ m^2 s^{-1} have generally been reported.[20,103] Xing et al. give:[92]

$$D_{\mathrm{O}_2,\mathrm{w}}/\mathrm{m}^2\ \mathrm{s}^{-1} = 7.4 \times 10^{-8} T \frac{\sqrt{2.6 M_{\mathrm{H_2O}} / 1\ \mathrm{kg\ mol}^{-1}}}{\mu_{\mathrm{w}} (V_{\mathrm{m,O}_2}/1\ \mathrm{m}^3)^{0.6}} \quad [49]$$

Various data for oxygen permeability in bulk membranes have also been presented as a function of water activity in the ionomer (Table III).

There is some disagreement related to how the ionomer-phase diffusivity, especially in ionomer thin films, compares to the bulk water value. Whereas Yoon et al. argue that $D_{\mathrm{O2,iono}}$ in thin films within an agglomerate is comparable to the liquid water value,[104] the above data as well as the results of Hao et al. suggest that it may be an order of magnitude slower within primary pores.[95,103] In bulk water, Gerteisen et al. give $D_{\mathrm{O2,w}} = 4.82 \times 10^{-9}$ m^2 s^{-1}.[87]

Table III. Measured values of oxygen permeability in Nafion 1100 membrane, as a function of water activity.

Source	a_w	$c_{eq,O2,iono}D_{O2,iono}$/mol m^{-1} s^{-1}
Suzuki et al.[94]	0.3	9.24×10^{-10}
Suzuki et al.[94]	0.6	1.37×10^{-9}
Suzuki et al.[94]	0.9	1.96×10^{-9}
Sethuraman et al.[174]	1	1.817×10^{-9}
Parthasarathy et al.[175]	1	7.7×10^{-10}

Macroscopically non-uniform catalyst layers.—Many researchers have investigated catalyst layers that are non-uniform across the macroscopic scale of the catalyst layer thickness—this may either be due to deliberate grading of the catalyst layer for performance enhancement, or to account for unintentional non-uniformity introduced through the process of manufacture. Such macroscopically non-uniform CLs are most easily expressed in a macro-homogeneous model using an explicit spatial dependence of the CL parameters. Systematic non-uniformity in properties such as agglomerate size and ionomer volume fraction has been proposed to arise during coating of the CL,[101] and has been demonstrated experimentally using high-resolution tomography.[105]

Springer et al. was the first work to consider graded distributions of composition of the CL.[35] Yoon et al. consider a case where the agglomerate particle radius varies linearly in the through-CL direction.[104] Wang et al. and Yin et al. have considered CLs with multiple discrete sub-layers in which ionomer volume fraction, overall porosity and agglomerate size are allowed to take distinct values.[56,106] Xing et al. consider a similar linear variation for a graded catalyst layer where multiple properties vary through the system.[107]

Two-phase Models of the Catalyst Layer

Liquid water and flooding.—Although the CL contains multiple phases (solids, ionomer, gas, liquid water, etc), it is common to use the terms "single-phase" and "two-phase" when referring to the treatment of water in the model. In a single-phase model, liquid water is not explicitly resolved. Conversely, in a two-phase model, the volume fraction of liquid water is described explicitly alongside the independent mass transfer and phase change phenomena of the liquid water phase. This is regularly considered a "flooding" condition—some part of the gas-phase volume fraction becomes blocked with liquid water. Since gas-phase reactant transport is generally rapid, while diffusion in the liquid water phase is similarly slow as in ionomer, flooding creates potentially severe transport limitations due to choking of reacting supply. In general, PEMFC design seeks to strike a careful balance in water management, such that sufficiently high hydration is maintained to ensure high proton conductivity in ionomer material, but not so high that significant flooding occurs through condensation within the CL. The occurrence of thin films of liquid water is noted in the CL, even at low water saturation;[82] these films may be highly spatially non-uniform.[108]

Conventional two-phase transport models used in PEMFC device simulation have been developed principally with a focus on the GDL and MPL components.[8,21,32,38,73,109–113] In these models, the liquid water content is not expressed as a concentration or effective density, but rather according to the liquid water saturation (s_l) as the dependent variable. Liquid water saturation is defined as the volume ratio of liquid water to total pore volume. In terms of s_l, the liquid water mass balance equation is:

$$\frac{\partial(\rho_w \varepsilon_{pore} s_l)}{\partial t} + \nabla\cdot\mathbf{J}_w = R_{m,w} \qquad [50]$$

This equation must be combined with an expression for the effective liquid water mass flux, $\mathbf{N}_{m,w}$. Among methods presented to date, the "two-fluid model" has emerged as prominent, in which a two-phase Darcy's law description for the gas and liquid water phases is combined with a defined functional expression of capillary pressure as a function of liquid water saturation;[114,115] its equations are summarised below. The principal alternative is the multiphase mixture (M^2) model, which simplifies the mathematical specification and implementation of the two-fluid model by imposing condensation-evaporation equilibrium throughout the PEMFC porous media.[116–118]

Several authors have remarked on the weaknesses of these standard models, due to their reliance on capillary pressure–saturation relationships with their origins in soil descriptions from Earth sciences[2,113,119]—these are not necessarily relevant model materials with respect to PEMFC porous media. The M^2 model has been explicitly criticised due to the absence of the necessary mass source terms relating to faradaic sources and sinks in the CL;[120] this statement has been disputed by proponents of the M^2 model,[121] and faradaic mass sources do indeed appear in practical implementations.[122]

To improve the applicability of two-fluid models to the CL, various researchers have attempted to access CL-specific capillary pressure–saturation relations,[123–125] but the occurrence of water sorption into the ionomer during water uptake experiments, concurrently with filling of CL pores, has been recognised to introduce significant ambiguity to the data analysis. Given the lack of agreement in the literature concerning two-phase models of GDL/MPL regions, the significantly increased complexity of CL morphology, as well as the presence of ionomer, casts further doubt on the overall quantitative suitability of two-fluid models.[103]

Some modelling approaches consider liquid water to fully flood the CL pores,[9,27] so that liquid water is explicitly present but two-phase phenomena are absent. In such models, the normally rapid gas-phase mass transport of the reacting species is absent, and so mass transport limitations arise macroscopically without a need for a microstructural model. For a flooded model including a mixture of water and ionomer, the diffusion of O_2 can be considered to occur in series through a thin ionomer film[9] according to Eq. 73, or in parallel through separate pathways in the water and ionomer phases.[54,100] Kulikovsky considered the case where an effective transport limitation is introduced through the electrolyte conductivity, while gas diffusion is considered to be infinitely fast.[72] Interfacial voids at the MPL-CL interface have been identified as locally saturated blocking sites to liquid water transport, especially under channel regions where compression is lower than under land;[126] in a macro-homogeneous model, this effect might be included as a lumped transport resistance at the interface.[127]

Mathematical treatment of flooding.—In a two-phase model, the influence of CL flooding must be accounted for by making the electrode kinetics and/or reactant transport somehow dependent on liquid water saturation.

In the absence of a microstructural model incorporating a saturation-dependent liquid water film, the standard approach to account for CL flooding is to assume that catalytic activity (local current density) scales polynomially with the volume fraction of pores still accessible to reactant transport in the gas phase:[24,115]

$$i_{ref} = i_{ref,0}(1 - s_l)^{n_{CL}} \qquad [51]$$

Here, $i_{ref,0}$ is the current density under dry conditions. The relation is widely assumed to be linear ($n_{CL} = 1$), but experimentally measured values have varied in the range $0.5 \leqslant n_{CL} \leqslant 0.62$.[128] This approach effectively treats reactants (H_2 or O_2) dissolved in liquid water as being inert at the liquid water–Pt interface, due to the absence of adequate proton conduction where the ionomer is absent.[129]

Liquid water saturation also makes paths for gas-phase diffusion more tortuous. A macroscopic tortuosity correction due to liquid water saturation in the CL has been suggested as follows:[36]

$$\frac{D_{eff,i,CL}}{D_i} = (1 - s_l)^{m_D}\left(\frac{\varepsilon_{pore} - \varepsilon_{crit}}{1 - \varepsilon_{crit}}\right)^{n_D} \qquad [52]$$

Wang et al. measured the gas-phase tortuosity in the CL, and proposed the following alternative expression:[130]

$$\frac{D_{\mathrm{eff},i,\mathrm{CL}}}{D_i} = (1 - s_\mathrm{l})^{m_D}\,\varepsilon_\mathrm{pore}^{n_D} \quad [53]$$

where the values of m_D and n_D depend on whether the diffusion model excludes Knudsen diffusion ($m_\mathrm{D} = n_\mathrm{D} = 4$) or includes it ($m_\mathrm{D} = n_\mathrm{D} = 5.5$).

The "conventional" two-fluid model.—The conventional two-fluid model is derived by applying Darcy's law to both gas and liquid phases, and then using a defined capillary pressure expression to constrain the relative values of the gas and liquid-phase pressures.

$$\mathbf{u}_\mathrm{g} = -\frac{\kappa_\mathrm{g}}{\mu_\mathrm{g}}\nabla p_\mathrm{g} \quad [54]$$

$$\mathbf{u}_\mathrm{l} = -\frac{\kappa_\mathrm{l}}{\mu_\mathrm{l}}\nabla p_\mathrm{l} \quad [55]$$

$$p_\mathrm{cap} = p_\mathrm{g} - p_\mathrm{l} \quad [56]$$

As noted previously,[21] the convention for PEMFC models is to define capillary pressure as Eq. 56, even in hydrophobic environments where liquid water becomes the non-wetting phase, and the value of p_cap becomes negative. By combining the above relations with a capillary pressure–saturation relation $p_\mathrm{cap}(s_\mathrm{l})$ and the conservation relation Eq. 50:[21,73]

$$\frac{\partial(\varepsilon_i s_\mathrm{l})}{\partial t} = \nabla\cdot(D_\mathrm{cap}\nabla s_\mathrm{l} - f_\mathrm{s}\,\mathbf{u}_\mathrm{g}) + \frac{R_\mathrm{w}}{\rho_\mathrm{w}} \quad [57]$$

$$f_\mathrm{s} = \frac{\kappa_\mathrm{l}}{\kappa_\mathrm{g}}\frac{\mu_\mathrm{g}}{\mu_\mathrm{l}} \quad [58]$$

$$D_\mathrm{cap} = -\frac{\kappa_\mathrm{l}}{\mu_\mathrm{w}}\frac{\partial p_\mathrm{cap}}{\partial s_\mathrm{l}} \quad [59]$$

Evaporation-condensation rate.—The distribution of gas-accessible pore sizes, and hence the transition between Knudsen diffusion of reacting gases and normal continuum diffusion, is influenced by the saturation degree. Performance decay is likely to appear due to rate limitation to evaporation-condensation processes.[131] Evaporation may occur more rapidly than in the GDL due to the small pore size in the CL, even with the difference in hydrophobicity. It has been suggested that evaporation can be as fast as the generation of water during the ORR for certain temperatures and pore size distributions.[132]

Most PEMFC simulations use the He equations to define the evaporation-condensation rate in the GDL (110):

$$R_\mathrm{m,w,g\to l} = k_\mathrm{c} M_\mathrm{H_2O} c_\mathrm{w,g}\frac{p_\mathrm{H_2O} - p_\mathrm{vap}}{p_\mathrm{A}},\ p_\mathrm{H_2O} > p_\mathrm{vap} \quad [60]$$

$$R_\mathrm{m,w,l\to g} = -k_\mathrm{v} M_\mathrm{H_2O} c_\mathrm{w,l}(p_\mathrm{vap} - p_\mathrm{H_2O}),\ p_\mathrm{H_2O} \leqslant p_\mathrm{vap} \quad [61]$$

$$c_\mathrm{w,g} = \varepsilon_\mathrm{pore}(1 - s_\mathrm{l})\frac{p_\mathrm{H_2O}}{RT} \quad [62]$$

$$c_\mathrm{w,l} = \varepsilon_\mathrm{pore} s_\mathrm{l}\frac{\rho_\mathrm{w}}{M_\mathrm{H_2O}} \quad [63]$$

Eikerling et al. proposed that the evaporation rate in the CL can be determined similarly, but using the critical capillary radius (see Eq. 68 below) to yield the implied gas-liquid interfacial volumetric surface area directly.[132]

$$R_\mathrm{w,l\to g,CL} = k_\mathrm{v,areal}\frac{\varepsilon_\mathrm{CL,dry}}{2r_\mathrm{crit}}(p_\mathrm{vap} - p_\mathrm{H_2O}) \quad [64]$$

The bulk expression of p_vap can be adapted to be suitable for the nanoscale composite environment of the CL, by using the Kelvin equation and an enthalpy change of vaporisation that is constant locally (ΔH_vap):

$$p_\mathrm{vap,app} = p_\mathrm{vap,0}\exp\left(\frac{-\Delta H_\mathrm{vap}}{RT}\right)\exp\left(p_\mathrm{cap}\frac{M_\mathrm{H_2O}}{RT\rho_\mathrm{w}}\right) \quad [65]$$

with $p_\mathrm{vap,0,CL} = 1.18 \times 106$ atm, $\Delta H_\mathrm{vap} \approx 43$ kJ mol^{-1}.[132]

Sorption to the CL ionomer component.—The presence of ionomer in the CL means that liquid water contributes to a sorption equilibrium that hydrates the ionomer, as well as participating in an evaporation-condensation equilibrium. Sorption in ionomers such as Nafion has been characterised to proceed differently under vapour- or liquid-equilibrated conditions (so-called Schröder's paradox);[20,32,57,58] as far as the distinction between the two types of sorption arises from structural interactions of the ionomer bulk and surfaces, the specific influence of liquid water regions may manifest differently in the case of ionomer thin films in the CL.[74,124] One suggested approach is to express water content in the CL ionomer as a direct multiple of its equivalent sorption isotherm in bulk ionomer.[94,125]

Water sorption causes swelling of the ionomer phase, which may reduce the CL pore volume. Shah et al. suggested accounting for this by the following linear relation:[86]

$$\varepsilon_\mathrm{iono} = \varepsilon_\mathrm{iono,0} + 0.0126\lambda \quad [66]$$

In the presence of multiple equilibria involving water in three phases (gas, liquid and ionomer), there is a risk that equilibrium specifications and boundary conditions may become inconsistent.[129] One preferential approach is to use only kinetic relations for each phase change, avoiding explicit equilibrium statements.[133] An alternative practical method for describing water balance from sorption mathematically in the case of partial liquid water saturation has been suggested by Olapade et al.[134]

Oxygen reduction reaction: product water in two-phase models.—When liquid water is explicitly resolved in the cathode catalyst layer, the faradaic mass source of water must be assigned to a phase. There is disagreement between different models on whether this product water is created as liquid water, as gas-phase water, or as water of hydration in the ionomer component of the CL. Sui et al. view product water as being introduced to "multiple phases simultaneously".[5] If evaporation-condensation equilibria are enforced in the CL, as in standard M^2 model formulations, the issue has no impact as the water will "automatically" find its thermodynamically correct phase. Likewise, the approach of enforcing uniform liquid- and gas-phase pressure in the CL will ensure that the appropriate phase is constrained.[32] In the presence of kinetically controlled evaporation and condensation, however, the choice may be impactful. A statistical review of the two-phase modelling literature suggests that defining product water in the liquid water phase is generally preferred.[21]

Relations from pore-size distribution analysis.—For a cylindrical pore of radius r_p and with a liquid-gas interface located somewhere along its length, the Young-Laplace equation gives its capillary pressure:

$$p_\mathrm{cap} = \frac{2\gamma}{r_\mathrm{p}}\cos\theta_\mathrm{c} \quad [67]$$

This relation has allowed the development of different theories of the capillary pressure–saturation relation using a statistical

distribution of pore sizes. It can be used to define a critical radius for pore imbibition as a function of the local capillary pressure:[32]

$$r_{crit} = \frac{2\gamma \cos\theta_c}{p_{cap}} \quad [68]$$

For the case of a hydrophilic pore, the critical radius, r_{crit}, is the smallest pore size filled, while for the case of a hydrophobic pore it corresponds to the largest pore size filled. In other models, the CL is divided on micropores, considered the primary pores with $r < 10$ nm and macropores considered the secondary pores with $r > 10$ nm; this bimodal pore-size distribution allows separation of wetting extent by pore radius.[132,135,136]

If the pore is filled up to the critical radius, the saturation can be defined as:[132]

$$s_l = \frac{1}{\varepsilon_{CL,dry}} \int_0^{r_{crit}} \frac{d\varepsilon_{CL}(r')}{dr'} dr' \quad [69]$$

Since the typical catalyst layer has a dual pore-size distribution, by convention it has been agreed that the composites are hydrophilic for $s_l < 0.7$ and hydrophobic for $s_l > 0.7$.[135] Within the pores, Strahl et al. assumed a thin water layer, and the ionomer was located on the micropores.[136] It is then assumed that the air pore is occupied by the liquid according to Eq. 68.

The volume occupied by the water in the primary pores is then the ratio of the pore not occupied by Pt or air. If the volume of the Pt particles is negligible and with a constant primary pore size r_{pp} of 10 nm, the primary pore saturation is given by:

$$s_{l,p} = 1 - \left(\frac{r_{crit}}{r_{pp}}\right)^3 \quad [70]$$

The combination of Eqs. 68 and 70 gives the following capillary pressure–saturation relation for the CL with only primary pores partially saturated:[136]

$$p_{cap} = \frac{2\gamma \cos\theta_{c,CL}}{r_{pp}(1 - s_{l,p})^{\frac{1}{3}}} \quad [71]$$

The volumetric electroactive area can be expressed as a function of the volume density of Pt particles $n_{vol,Pt}$ and a curvature length scale h_s:[136]

$$a_{CL} = n_{vol,Pt} 2\pi r_{Pt} \max(h_s + r_{pp}(1 - s_{l,p})^{\frac{1}{3}}, 2r_{Pt}) \quad [72]$$

For secondary pores, an analogous formula was derived, with a secondary pore radius r_{ps} to extend Eq. 71 to s_l where primary pores are completely saturated.

Microstructural Models

Influence of CL microstructure.—Since O_2 diffusion in ionomer is generally much slower than in the gas-phase, it is not normally relevant to consider ionomer-phase diffusion in the macroscale dimension. Instead, it is only important to consider the rate of diffusion in the nanoscale dimension of the ionomer film coating the electrocatalyst.

The simplest model of O_2 diffusion through the ionomer within the CL microstructure that is nonetheless capable of predicting transport losses is the assumption of linear diffusion through a thin ionomer film of defined thickness, with thermodynamic equilibrium with the gas-phase (concentration $c_{eq,O2}$) at the outer surface of the thin film:[9,83,137,138]

$$R_{diff,O_2} = -a_{CL} \frac{D_{O_2,iono}}{d_{film}} (c_{eq,O_2} - c_{O_2,agg}) \quad [73]$$

where $c_{O2,agg}$ represents the oxygen concentration in the ionomer at an active particle (in an agglomerate model, at the outer radius of the agglomerate particle). This concentration could be determined self-consistently by treating $c_{O2,agg}$ as the relevant oxygen concentration in an electrode kinetic model predicting $R_{far,O2}$, and requiring equality of the latter with the diffusion-limited quantity in Eq. 73.

Even in the absence of any more detailed microstructural model, the mass transport limitation given by Eq. 73 has been described as a key overlooked phenomenon in simpler macro-homogeneous models.[23] A fuller alternative is to develop a more detailed agglomerate model; common approaches are based on the assumption of a homogenised composite of electronic conductor with electrocatalyst, clad in spherical shells of liquid water and/or ionomer.[139–141]

Characterisation of microstructural morphology.—Characterization of the catalyst layer through SEM and nanoscale X-ray computed tomography (nano-CT) has revealed that the internal morphology is complex and heterogeneous at multiple length scales. Cetinbas et al. used nano-CT, small and ultra-small angle X-ray scattering (SAXS and USAXS respectively), TEM and porosimetry to affirm the common understanding that the loaded Pt/C forms agglomerates of several carbon particles.[105] The individual Pt nanoparticles have sizes of 2–10 nm. These decorate the surfaces of the carbon black support particles with sizes of 20–70 nm, which form agglomerates of diameter typically in the range of 100–400 nm. Cetinbas et al. used their result to reconstruct typical agglomerates (Fig. 4).

The presence of the ionomer as a coating (thin film) on the agglomerate particles is also a prediction of coarse-grained molecular dynamics simulations.[142] Interactions with Pt nanoparticles as well as the very low thickness of the coating means that the properties of such a nanoscale film are likely to be appreciably different from those of bulk ionomer.

Sizes of the primary pores (microporosity) within each agglomerate are typically quoted as < 10 nm[1]. The secondary pores between agglomerate particles were reported as having sizes up to 50 nm in earlier studies,[1,132] while later work reported a range 60–180 nm across mean values from three studies,[102] and 150 nm has been assumed as reasonable elsewhere.[143] Of course, the precise distribution of any sample will depend upon specific materials and preparation method.

Within agglomerates, the uniformity of distribution of Pt catalyst is uncertain. Darling et al.[143] suggested that materials with low microporosity, such as Vulcan, do not allow Pt to penetrate the carbon agglomerates effectively, so that a large amount of Pt is close to the secondary pores. Conversely, materials with high microporosity, such as TEC10V50E may show more uniform Pt distribution.

Eikerling et al. proposed a bimodal pore size distribution for pore radius r_p:[132]

$$d\varepsilon_{CL} = dr_p \frac{\varepsilon_{pore}}{\sqrt{\pi}(\ln s_{pp} + \chi_{ps} \ln s_{ps})} \frac{1}{r_p}$$

$$\left(\exp\left(-\left(\frac{\ln\left(\frac{r_p}{r_{pp}}\right)}{\ln s_{pp}} \right)^2 \right) + \chi_{ps} \exp\left(-\left(\frac{\ln(r_p/r_{ps})}{\ln s_{ps}} \right)^2 \right) \right) \quad [74]$$

Here, subscript "pp" represents primary pores and subscript "ps" represents secondary pores. χ_{ps} is a relative contribution of secondary pores. r_i and s_i are positions of peak maxima and their respective peak widths in the distribution. One proposed simplification of this distribution is a bimodal delta distribution, in which porosity is distributed between two types of pores, each with uniform size.

Agglomerate models.— *Historical development and criticism of agglomerate models.*—Based on the morphological observations summarised above, many works have worked towards "agglomerate models" in which the influence of this microstructural arrangement

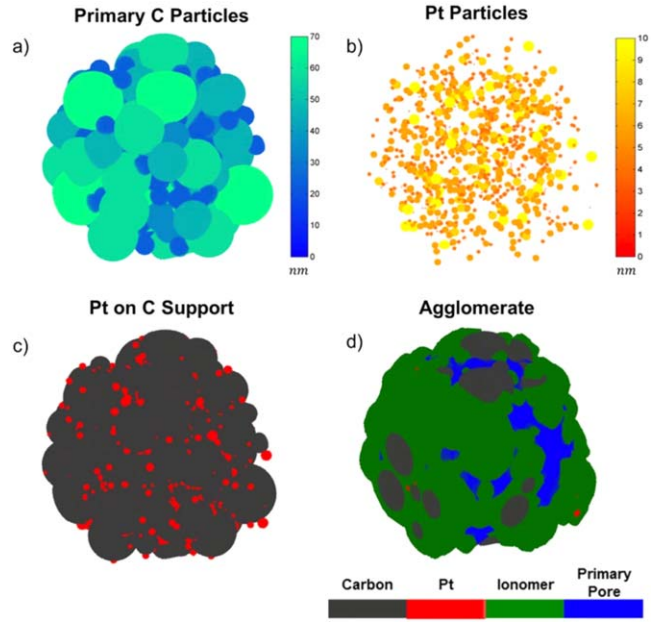

Figure 4. Reconstruction of a typical agglomerate according to Cetinbas et al.[105] (a) carbon particles, (b) Pt particles, (c) Pt particles on carbon support, and (d) fully assembled agglomerate. Reproduced by permission of IOP Publishing Ltd All rights reserved.

is accounted for analytically. The conventional agglomerate model assumes spherical agglomerate particles with a uniform radius r_{agg}, where each particle contains a homogeneous distribution of active Pt and is fully flooded with ionomer. Alternatively, water may be the flooding material—in either case, there is no gas-phase penetration of the agglomerate.[140,144] It is common to consider a thin film of ionomer to form a concentric spherical shell coating the outer surface of the agglomerate. Liquid water, where present, is then treated as a further concentric layer of defined thickness—i.e., water is filling secondary pores in the CL structure.

A historical review of agglomerate models has been given by Yuan et al.[139] A very wide range of agglomerate radii and ionomer film thicknesses have been used in the literature; these values have recently been tabulated and scrutinised.[140,141] Agglomerate models became especially popular in the 2000s, and were argued at that time to be essential to reproduce experimentally observed transport limitations at higher current densities.[145] It has been argued that the finite kinetics of O_2 dissolution in ionomer (expressed by Eq. 44) can account for many of the same phenomena as agglomerate models.[94] Considering criticism of the latter work,[96] the status seems to be uncertain. A moderate consensus is progressively emerging whereby the inputs to the agglomerate model are seen as effectively constituting additional fitting parameters that are capable of (empirically) quantifying microscale transport limitations in the catalyst layer, and thus the agglomerate is a phenomenological rather than realistic description of CL microstructure.[74,146]

For some conditions, the transport limitation due to the thin film has been argued to dominate the transport limitation in the interior of the agglomerate particle.[52,85,147] This is especially the case if the reactant activity in the interior of the agglomerate is negligible,[86] since otherwise the smaller thickness of the ionomer film should make its contribution to the overall Thiele modulus small (see Eq. 81 below). Like the agglomerate particle radius itself, the ionomer film thickness has been criticised as an experimentally uncertain parameter.[145] More recently, experimental evidence has also been given to suggest that the ionomer film is incomplete.[140] Works excluding the ionomer film have shown negligible transport losses in a spherical agglomerate for typical experimentally observed agglomerate sizes,[95,148] and the experimental observation of catalyst layer-dependent transport limitations does suggest that some consideration of the microstructure is needed.

Although most authors consider the spherical agglomerate to be fully flooded with either ionomer or water, Yin et al. considered the case of a partially flooded agglomerate, including a variation in gas-phase O2 concentration due to nanoporous diffusion from the agglomerate outer radius to the outer radius of the flooded region.[149] This type of structure has apparently not been considered subsequently. Das et al. developed a model based on Bruggeman theory in which the catalyst layer can be viewed as a dispersion of agglomerate particles clad in further concentric spheres of air and/or water;[150] this approach simplifies the determination of effective macro-homogeneous transport properties, but may not be consistent with the real material connectivity. Pisani et al. considered the spherical unit cell of agglomerates surrounded by air, and argued that a sufficiently high gas porosity is required for the spherical agglomerate model to be meaningful—otherwise, secondary pores lack the connectivity required to consider a homogeneous distribution of oxygen concentration.[42]

The penetration of the agglomerate microporosity by ionomer has been argued against based on the pore sizes (< 10 nm).[140,144] The absence of ionomer content in the agglomerate interior could render it chemically inactive, making the ionomer film the important feature;[52] alternatively, proton transport in water in the agglomerate interior could be significant.[140] The free proton conductivity in water in nanopores has been argued as negligible, on the basis that these pores are comparable in size to open channels in ionomer material.[56,151] Huang et al. also argued that the low number of C nanoparticles in a typically sized agglomerate challenge the assumption of continuity.[140]

Xing et al. considered the primary pores of the agglomerate particle as a generalised void space that may be filled with ionomer or water, or dry gas.[90] However, this model did not consider microstructural interactions due to the different components, and instead simply weighted the spherical agglomerate equation. Work from the same authors has also considered the primary pores to contain an ionomer-gas mixture, while a liquid water film is present on the agglomerate surface.[92] This concept does not seem to match closely with the reported morphology from experiment.

Some other authors have considered the catalyst layer in terms of parallel cylindrical gas pores with a coating of agglomerate material on the pore walls;[152] however, this is not more descriptive of the real microstructure and does not seem to make it more straightforward to parameterise the system. Jain et al. reviewed the influence of different Thiele moduli as implied by different possible agglomerate geometries.[153] Nonequilibrium phenomena in cylindrical gas pores were considered in terms of a two-scale microstructural model by Kulikovsky.[154]

Formulation of the standard agglomerate model.—Assuming that all ionomer is present either within the agglomerate, or as a thin film of thickness d_{film} on the agglomerate surfaces, the volume fractions are controlled by the properties of the catalyst ink:[26]

$$\varepsilon_{iono} = \varepsilon_{agg}\left(\varepsilon_{iono,agg} + \left(1 + \frac{d_{film}}{r_{agg}}\right)^3 - 1\right) \quad [75]$$

If $\varepsilon_{iono,agg}$, the volume fraction of ionomer in the agglomerate phase within the film, is used as an input parameter, the film thickness can be expressed from the ionomer content according to Eq. 75 as:

$$d_{film} = r_{agg}\left(\left(1 + \frac{\varepsilon_{mem}}{\varepsilon_{agg}} - \varepsilon_{mem,agg}\right)^{\frac{1}{3}} - 1\right) \quad [76]$$

where the ionomer and agglomerate volume fractions are computed from the loading according to Eqs. 4 and 5.

In a spherical agglomerate model, the interfacial surface area a_{agg} inside the ionomer film can be defined from the agglomerate radius:

$$a_{agg} = \frac{3\varepsilon_{agg}}{r_{agg}}(1 - \gamma_{inact}) \quad [77]$$

where γ_{inact} is the blocked proportion of the surface area due to incomplete coverage of ionomer film.[23]

By defining an active interfacial area of Pt per unit volume of agglomerate particle, a volumetric reaction source/sink for the H_2 and O_2 can be defined and solved as the source term of a spherical diffusion equation with a thermodynamically (or kinetically) controlled concentration of dissolved gas at the outer surface of the agglomerate. Given the typical scale of an agglomerate particle, the electrical and electrolyte potentials as well as temperature are usually treated as uniform within the particle,[104] so that the electrochemical driving force for the reaction (including activation overpotential) depends only upon the distribution of reactant concentration.

With these simplifying assumptions and assuming a first-order, irreversible reaction, the macro-homogeneous reaction source can be defined as follows, if the ionomer film surrounding the agglomerate is ignored:[155]

$$R_{far,O_2} = -k_{agg}\varepsilon_{agg}\xi c_{O_2,agg} \quad [78]$$

The effective volumetric rate constant k_{agg} (s^{-1}) is given:

$$k_{agg} = \frac{i_{act}}{4Fc_{O_2,ref}}a_{CL}\varepsilon_{iono,agg} \quad [79]$$

ξ is the agglomerate effectiveness factor defined from a corresponding Thiele modulus and $i_{0,act,i}$ is the concentration-independent part of the kinetic rate law.[19]

For a spherical agglomerate and a linear reaction:

$$\xi = 3\left(\frac{\coth\beta_T}{\beta_T} - \frac{1}{\beta_T^2}\right) \quad [80]$$

where the Thiele modulus β_T is in turn given as:

$$\beta_T = r_{agg}\sqrt{\frac{k_{agg}}{D_{eff,O_2,agg}}} \quad [81]$$

Many authors use the Bruggeman relation for O_2 diffusivity within the nanopores of the spherical agglomerate, while using bulk diffusivity in a surrounding ionomer film:[59,88,89,149,156]

$$D_{eff,O_2,agg} = \varepsilon_{iono,agg}^{3/2}D_{O_2,iono} \quad [82]$$

The spherical flooded agglomerate model can be extended by including a thin film of ionomer at the outer radius of the agglomerate particle, which acts as an additional transport barrier.[25,44,83] In practice, this means that Eq. 78 is combined with the film mass transport Eq. 73, eliminating the agglomerate concentration. The overall approach yields:[44,85]

$$R_{far,O_2} = -\varepsilon_{agg}c_{O_2,agg}\left(\frac{1}{k_{agg}\xi} + \frac{r_{agg}^2}{3D_{O_2,iono}}\left(\frac{d_{film}}{r_{agg} + d_{film}}\right)\right)^{-1} \quad [83]$$

Note that the precise formulation of Eq. 83 varies between different references due to the specific choice of definition of ε_{agg}, which in some cases includes the volume of the ionomer film on the agglomerate surface, and in some cases does not.

Two-phase agglomerate models.—Some authors consider the combination of an agglomerate model with specifically two-phase transport in the CL to be essential to reproduce experimental data accurately.[23,157] The parameterisation and parameter sensitivity of two-phase agglomerate models has been studied extensively by Li et al.[141] One route to account for liquid water is to define a liquid water film thickness outside the ionomer thickness occurring in Eq. 76, assuming that all liquid water is present as a thin (quasi-planar) liquid water layer, on the agglomerate particles:

$$d_w = \frac{s_1\varepsilon_{pore}}{a_{agg}} \quad [84]$$

where a_{agg} is the volumetric surface area of the agglomerate. Schwarz et al. allowed a direct definition of a_{agg} from a specified film thickness:[103]

$$a_{agg} = \frac{\varepsilon_{agg}}{d_{film}} \quad [85]$$

In "wet gas" models, for which liquid water is represented as a gas-phase mass fraction rather than as a distinct phase, the liquid water concentration can be used in place of the saturation to define a thin water film in a similar manner.[158]

If the water in the CL occurs in the film, the film thickness the depends on the saturation and particle properties. The gas reactants must dissolve and diffuse through the film to be able to find a site for reaction; this adds a transport limitation that is saturation dependent. The gas solubility in the film may also be different than in the ionomer.[159]

In other models, cylindrical agglomerates are combined with the water film, assuming that the ionomer phase is saturated with water.[152] They also express the film thickness assuming a thin liquid water layer as in Eq. 84.

The same thin-film approach has been applied subsequently in combination with an experimentally measured capillary pressure-saturation relation for the CL,[160] and has been applied to the spherical geometry also.[23,161]

A rigorous combination of the agglomerate model with a two-phase CL model was introduced for the spherical agglomerate geometry by the Shah group.[86] The water film thickness is expressed as a function of the agglomerate properties as:

$$d_w = (r_{agg} + d_{film})\left(\left(1 + \frac{3s_1\varepsilon_{pore}}{4\pi n_{vol,agg}(r_{agg} + d_{film})^3}\right)^{\frac{1}{3}} - 1\right) \quad [86]$$

This formula contained an error in the second term in the original publication,[86] which was corrected subsequently.[159] $n_{vol,agg}$ represents the number of agglomerates per unit dry material volume. Writing

$$n_{vol,agg} = \frac{\varepsilon_{agg}}{\frac{4\pi}{3}r_{agg}^3(1 - \varepsilon_{pore})} \quad [87]$$

yields a corresponding expression for film thickness as:[92]

$$d_w = (r_{agg} + d_{film})\left(\left(1 + \frac{s_1\varepsilon_{pore}(1 - \varepsilon_{pore})}{\varepsilon_{agg}}\left(\frac{r_{agg}}{r_{agg} + d_{film}}\right)^3\right)^{\frac{1}{3}} - 1\right) \quad [88]$$

A different expression has been given by Jo et al.,[162] but the latter is either simply in error, or else the assumptions or definitions leading to its derivation are not clearly expressed. In the thin film limit, using linear rather than spherical diffusion (i.e. assuming a quasi-planar thin film), Schwarz et al. wrote more simply:[103]

$$d_w = \frac{\varepsilon_{pore} s_l}{\varepsilon_{iono}} d_{film} \quad [89]$$

Extensions to the standard agglomerate model.—The derivation of a Thiele modulus is more complex for the case of non-integer reaction order, or if the reaction is considered at all reversible. Both concerns may apply to the HOR. Mechanistically detailed descriptions of the ORR also display nonlinear apparent reaction order and may be challenging to combine with an agglomerate model.[59,163–165]

Proton concentration is usually considered to be constant within the agglomerates, but Nernst-Planck transport models have also been implemented to allow variable proton concentration as well as to study other variable conditions at the microscale.[59,86,166] Moore et al. used an extra 1D dimension for the agglomerate radius, in which proton transport is described using an electrolyte potential according to an Ohm's law model;[59] this model allows overpotential to vary through the agglomerate due to non-ideal proton transport.

Diffuse and compact double layer phenomena have been considered within the agglomerate model for EIS calculations of the catalyst layer,[167] but since these phenomena manifest only at sub-ms timescales, they can be excluded for normal transient or steady-state calculations of the CL.[40]

Significant differences may exist in predictions between an agglomerate model with a unique, uniform agglomerate radius, and a model introducing a volumetric weighting across an experimentally determined distribution of agglomerate sizes.[168] Such a weighting can be expressed as:

$$i_{v,loc} = \int_0^\infty i_{v,loc}(r_{agg})\, P_{vol}(r_{agg})\, dr_{agg} \quad [90]$$

Alternatives to the agglomerate model.—Given that microstructural detail is usually difficult to quantify for a real catalyst layer, Weber et al. proposed the expression of a single mass transfer characteristic φ_{mt}.[24] In terms of a phenomenological interpretation of the agglomerate model, this mass transfer characteristic correlates to the agglomerate Thiele modulus as follows:

$$\beta_T = \sqrt{\frac{k_m c_{m,ref} \phi_{mt,m}}{p_{m,ref}}} \quad [91]$$

Suggested values are: $\varphi_{mt,a} = 8 \times 10^{-3}$ bar m^3 s mol^{-1}, $\varphi_{mt,c} = 6 \times 10^{-3}$ bar m^3 s mol^{-1}.

Khajeh-Hosseini-Dalasm et al. ignored microstructure because of perceived imprecision in the measurement and definition of size, shape and composition of agglomerate particles.[27] Instead, this work considers the CL with liquid water fully flooding the void space, and pure ionomer and GDL phases penetrating a finite distance into the CL. This work defined an arbitrary cylindrical control volume in which a Pt/C particle sits in the centre and the other phases surround it with an angular distribution according to their volume fraction; O_2 diffuses in the radial direction through both ionomer and void (liquid water) regions. This radial mass transport model has subsequently been extended to consider parallel access to reaction sites by transport through ionomer, liquid water, and gas, with uniquely defined O_2 mass transfer resistances in each medium, and a weighting according to the volume fraction.[54]

Discrete Pt particle effects.—The analysis of specific interactions with discrete Pt particles is complicated by the continuing uncertainty regarding the phase from which electron transfer takes place at the Pt interface. Some authors have considered electron transfer at the Pt-ionomer interface to be more probable;[138] other works argue that if the catalyst layer is humidified sufficiently, no such interface exists, and electron transfer takes place at a Pt-water interface.[140]

In general, the random nature of catalyst layer manufacture results in poor utilisation of the Pt catalyst.[1] Eikerling et al. used percolation theory to correct the electroactive surface area to account for the effective accessible volume of the three-phase contacts:[55]

$$a_{CL,eff} = a_{CL} P(\varepsilon_{iono}) P(\varepsilon_{agg})((1 - \chi_{res})(1 - (1 - P(\varepsilon_{gas}))^M) + \chi_{res}) \quad [92]$$

while Wang et al. sets:[56]

$$a_{CL,eff} = a_{CL} P(\varepsilon_{mem}) P(\varepsilon_{agg})((1 - \chi_{res})(1 - (1 - P(\varepsilon_{gas}))^M) + \chi_{res}(1 - P(\varepsilon_{gas}))^M) \quad [93]$$

with $M = 4$. χ_{res} is a residual active area (value not given, but suggested < 0.2 in[55]), and:

$$P(\varepsilon_m) = \frac{\varepsilon_m}{(1 + \exp(-a(\varepsilon_m - \varepsilon_{crit})))^b} \quad [94]$$

with $a = 53.7$ and $b = 3.2$.

The classical agglomerate model includes the effect of Pt loading on the apparent transfer resistance of the catalyst layer only in terms of the electroactive area a_{CL}, which is assumed to simply scale the apparent kinetic rate constant for the agglomerate according to a homogeneous distribution of Pt. Experimentally, the effective transport resistance has been observed to increase nonlinearly at low Pt loading; see Fig. 5.[143] Several authors have rationalised this observation in terms of the incomplete overlap of diffusion domains associated with individual Pt nanoparticles within the ionomer.[9,104]

In a spherical flooded film-agglomerate model where both ionic potential and oxygen concentration vary within the agglomerate, Yoon et al. demonstrated that a significantly lower relative current density is delivered in the presence of sparse active reaction sites (sparse Pt particles).[104] This theory has been generalised in terms of a Pt loading-dependent effective diffusion length for O_2 passing through the ionomer film, without requiring a specific agglomerate model.[95]

One recent study considered the case of partial ionomer film coverage, with liquid water flooding the agglomerate.[173] This study also considered mass transport limitations in the local spherical coordinate system of an individual Pt particle, to account for cases where Pt loading is sparse on the ionomer scale; to fit experiment, a much lower O_2 permeability compared to bulk was required both for the liquid water and ionomer.

Nanoscale transport to an individual Pt sphere was combined by Darling et al. with an adsorption kinetics barrier between the ionomer and the Pt surface, to adapt the Thiele modulus as follows:[143]

$$\beta_{T,Pt} = \beta_T \sqrt{\frac{1}{1 + \beta_{Pt}}} \quad [95]$$

$$\beta_{Pt} = \frac{k_{agg}}{a_{CL} \varepsilon_{iono,agg}} \left(\frac{d_{Pt}}{D_{eff}} + \frac{1}{k_{ads,Pt}} \right) \quad [96]$$

where $\beta_{T,Pt}$ is then used in place of β_T in Eq. 80. d_{Pt} is the individual Pt particle diameter (m) and $k_{ads,Pt}$ is the adsorption rate constant for O_2 on Pt (m s^{-1}).

Summary and Concluding Remarks

Compared to other works, which discuss how different models are implemented or which focus on specific details of the CL, we have collated the essential equations proposed in the literature up to 2022 to simulate PEMFC catalyst layers. Most of the work has focused on the cathode catalyst layer, since the slow rate of the ORR compared to the HOR causes the cathode to exhibit a much greater activation loss, although some examples for the anode were also noted when appropriate. We have focused our attention on

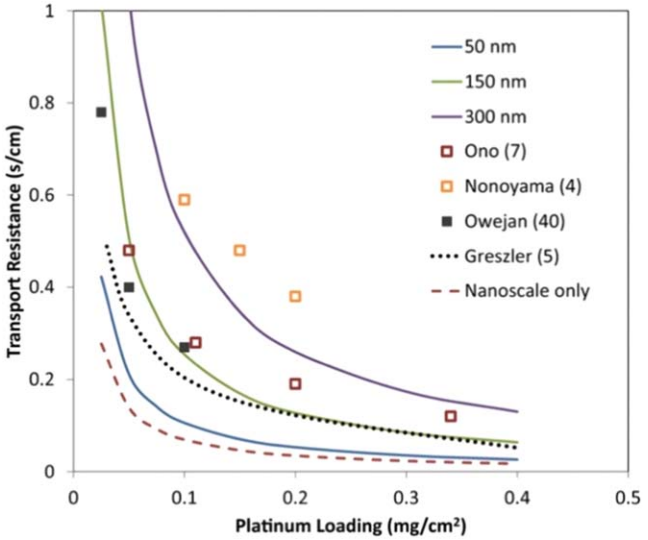

Figure 5. Experimental and predicted effective transport resistance in the ionomer as a function of platinum loading and comparison to the works of Ono et al.,[169] Nonoyama et al.,[170] Owejan et al. [171] and Greszler et al.[172] Obtained from.[143]

differences between the models to highlight their advantages and where there is a lack of agreement between research groups. For example, the thin-film and macro-homogeneous models of the catalyst layer composition were reviewed and compared with each other; both these models allow homogenised descriptions of the detailed morphology of the catalyst layer, but the former is preferred when transport losses can be ignored. Different regularly used electrode kinetic expressions were discussed, emphasising that for common operating conditions, reported complex kinetic formulations do not offer any significant advantage over simpler treatments. A lack of consistency in reported O_2 diffusivity through the ionomer phase was raised; however, this has been explained by the insensitivity of the response to this property, due to the dominance of the gas-phase mass transport at the microscale and the correlated uncertainty in ionomer film thickness at the nanoscale. Nanoscale transport limitations for oxygen in the ionomer and/or liquid water phase within the cathode catalyst layer have been implicated as key contributors to the observation of a transport-limited current. There is not yet agreement, however, on the most appropriate physical model for describing this phenomenon; detailed agglomerate models in vogue in the 2000s are increasingly viewed as adding no true physical insight. Overall, we believe that our work will allow researchers to make a more informed decision when selecting the appropriate model for their CL.

Acknowledgments

This work was funded by the National Measurement System of the UK Department of Science, Innovation and Technology. Andy Wain, Graham Smith, and Gareth Hinds (National Physical Laboratory, Teddington, UK) provided helpful comments on the text.

ORCID

Edmund J. F. Dickinson https://orcid.org/0000-0003-2137-3327
Oliver Rodríguez https://orcid.org/0000-0003-2350-1214

References

1. B. Andreaus and M. Eikerling, *Device and Materials Modeling in PEM Fuel Cells*, **113**, 41 (2009).
2. S. Balasubramanian and A. Z. Weber, *Physical Multiscale Modeling and Numerical Simulation of Electrochemical Devices for Energy Conversion and Storage: From Theory to Engineering to Practice*, ed. A. A. Franco et al. (Springer, London) 91 (2016).
3. S. Tzelepis, K. A. Kavadias, G. E. Marnellos, and G. Xydis, *Renewable Sustainable Energy Rev.*, **151**, 111543 (2021).
4. Y. Chen, Y. Liu, Y. Xu, X. Guo, Y. Cao, and W. Ming, *Coatings*, **12**, 1145 (2022).
5. P. C. Sui, X. Zhu, and N. Djilali, *Electrochemical Energy Reviews*, **2**, 428 (2019).
6. M. Prokop, M. Drakselova, and K. Bouzek, *Current Opinion in Electrochemistry*, **20**, 20 (2020).
7. V. Novák, M. Dudák, P. Kočí, and M. Marek, *Current Opinion in Chemical Engineering*, **9**, 16 (2015).
8. M. Andersson, S. B. Beale, M. Espinoza, Z. Wu, and W. Lehnertbe, *Appl. Energy*, **180**, 757 (2016).
9. C. Marr and X. Li, *J. Power Sources*, **77**, 17 (1999).
10. N. P. Siegel, M. W. Ellis, D. J. Nelson, and M. R. von Spakovsky, *J. Power Sources*, **115**, 81 (2003).
11. K. Z. Yao, K. Karan, K. B. McAuley, P. Oosthuizen, B. Peppley, and T. Xie, *Fuel Cells*, **4**, 3 (2004).
12. J. R. De Lile and S. Zhou, *Electrochim. Acta*, **177**, 4 (2015).
13. M. Shojayian and E. Kjeang, *J. Power Sources*, **591**, 233820 (2024).
14. Z. Liu, Z. Mao, C. Wang, W. Zhuge, and Y. Zhang, *J. Power Sources*, **160**, 1111 (2006).
15. Y. Zhang, S. He, X. Jiang, X. Yang, Z. Wang, S. Zhang, J. Cao, H. Fang, and Q. Li, *Appl. Energy*, **357**, 122507 (2024).
16. J. A. Salva, A. Iranzo, F. Rosa, and E. Tapia, *Int. J. Hydrogen Energy*, **41**, 20615 (2016).
17. G. B. Zhang and K. Jiao, *J. Power Sources*, **391**, 120 (2018).
18. T. Tsukamoto, T. Aoki, H. Kanesaka, T. Taniguchi, T. Takayama, H. Motegi, R. Takayama, S. Tanaka, K. Komiyama, and M. Yoneda, *J. Power Sources*, **488**, 229412 (2021).
19. E. J. F. Dickinson and G. Hinds, *J. Electrochem. Soc.*, **166**, F221 (2019).
20. E. J. F. Dickinson and G. Smith, *Membranes*, **10**, 310 (2020).
21. E. J. F. Dickinson, "Review of Methods for Modelling Two-Phase Phenomena in a Polymer Electrolyte Membrane Fuel Cell (PEMFC)." *National Physical Laboratory MAT 93* (2020).
22. A. Kneer and N. Wagner, *J. Electrochem. Soc.*, **166**, F120 (2019).
23. R. M. Rao, D. Bhattacharyya, R. Rengaswamy, and S. R. Choudhury, *J. Power Sources*, **173**, 375 (2007).
24. A. Z. Weber and J. Newman, *J. Electrochem. Soc.*, **152**, A677 (2005).
25. Y. Bultel, P. Ozil, R. Durand, and D. Simonsson, *Electrochemical Society Proceedings*, **95**, 34 (1995).
26. M. Secanell, K. Karan, A. Suleman, and N. Djilali, *Electrochim. Acta*, **52**, 6318 (2007).
27. N. Khajeh-Hosseini-Dalasm, M. J. Kermani, D. G. Moghaddam, and J. M. Stockie, *Int. J. Hydrogen Energy*, **35**, 2417 (2010).
28. F. C. Cetinbas, S. G. Advani, and A. K. Prasad, *J. Electrochem. Soc.*, **161**, F803 (2014).
29. T. E. Springer, T. A. Zawodzinski, and S. Gottesfeld, *J. Electrochem. Soc.*, **138**, 2334 (1991).
30. T. Berning, D. M. Lu, and N. Djilali, *J. Power Sources*, **106**, 284 (2002).
31. B. R. Sivertsen and N. Djilali, *J. Power Sources*, **141**, 65 (2005).
32. A. Z. Weber, R. M. Darling, and J. Newman, *J. Electrochem. Soc.*, **151**, A1715 (2004).
33. E. Nishiyama and T. Murahashi, *J. Power Sources*, **196**, 1847 (2011).
34. D. M. Bernardi and M. W. Verbrugge, *J. Electrochem. Soc.*, **139**, 2477 (1992).
35. T. E. Springer, M. S. Wilson, and S. Gottesfeld, *J. Electrochem. Soc.*, **140**, 3513 (1993).
36. M. Eikerling and A. A. Kornyshev, *J. Electroanal. Chem.*, **453**, 89 (1998).
37. S. Um, C.-Y. Wang, and K. S. Chen, *J. Electrochem. Soc.*, **147**, 4485 (2000).
38. C.-Y. Wang, *Chem. Rev.*, **104**, 4727 (2004).
39. J. Newman and W. Tiedemann, *AIChE J.*, **21**, 25 (1975).
40. Y. Wang and C.-Y. Wang, *Electrochim. Acta*, **50**, 1307 (2005).
41. R. M. Rao and R. Rengaswamy, *J. Power Sources*, **158**, 110 (2006).
42. L. Pisani, M. Valentini, and G. Murgia, *J. Electrochem. Soc.*, **150**, A1549 (2003).
43. C. Boyer, S. Gamburzev, O. Velev, S. Srinivasan, and A. J. Appleby, *Electrochim. Acta*, **43**, 3703 (1998).
44. F. Jaouen, G. Lindbergh, and G. Sundholm, *J. Electrochem. Soc.*, **149**, A437 (2002).
45. D. A. G. Bruggeman, *Ann. Phys.*, **416**, 636 (1935).
46. B. Tjaden, S. J. Cooper, D. J. L. Brett, D. Kramer, and P. R. Shearing, *Current Opinion in Chemical Engineering*, **12**, 44 (2016).
47. B. Tjaden, D. J. L. Brett, and P. R. Shearing, *Int. Mater. Rev.*, **63**, 47 (2018).
48. G. Wang, P. P. Mukherjee, and C.-Y. Wang, *Electrochim. Acta*, **51**, 3139 (2006).
49. G. Wang, P. P. Mukherjee, and C.-Y. Wang, *Electrochim. Acta*, **51**, 3151 (2006).
50. P. K. Das, X. G. Li, and Z. S. Liu, *J. Power Sources*, **179**, 186 (2008).
51. C. Y. Jung, C. H. Park, Y. M. Lee, W. J. Kim, and S. C. Yi, *Int. J. Hydrogen Energy*, **35**, 8433 (2010).
52. Y. Tabe, M. Nishino, H. Takamatsu, and T. Chikahisa, *J. Electrochem. Soc.*, **158**, B1246 (2011).
53. D. Fofana, J. Hamelin, and P. Benard, *Int. J. Hydrogen Energy*, **38**, 10050 (2013).
54. H. Heidary, M. J. Kermani, and N. Khajeh-Hosseini-Dalasm, *Int. J. Hydrogen Energy*, **41**, 22274 (2016).
55. M. Eikerling, A. S. Ioselevich, and A. A. Kornyshev, *Fuel Cells*, **4**, 131 (2004).
56. Q. P. Wang, M. Eikerling, D. T. Song, Z. S. Liu, T. Navessin, Z. Xie, and S. Holdcroft, *J. Electrochem. Soc.*, **151**, A950 (2004).
57. A. Z. Weber and J. Newman, *J. Electrochem. Soc.*, **150**, A1008 (2003).
58. A. Z. Weber and J. Newman, *J. Electrochem. Soc.*, **151**, A311 (2004).

59. M. Moore, P. Wardlaw, P. Dobson, J. J. Boisvert, A. Putz, R. J. Spiteri, and M. Secanell, *J. Electrochem. Soc.*, **161**, E3125 (2014).
60. U. Reimer, Y. Cai, R. Li, D. Froning, and W. Lehnert, *J. Electrochem. Soc.*, **166**, F3098 (2019).
61. S. Gottesfeld and T. A. Zawodzinski, *Advances in Electrochemical Science and Engineering*, ed. R. C. Alkire et al. (Wiley, New York) (1997).
62. C. J. Song, Y. H. Tang, J. L. Zhang, J. J. Zhang, H. J. Wang, J. Shen, S. McDermid, J. Li, and P. Kozak, *Electrochim. Acta*, **52**, 2552 (2007).
63. F. Barbir, *PEM Fuel Cells: Theory and Practice* (Academic, Waltham, MA) (2013).
64. A. R. Kucernak and C. Zalitis, *J. Phys. Chem. C*, **120**, 10721 (2016).
65. J. Wang, T. Springer, and R. Adzic, *J. Electrochem. Soc.*, **153**, A1732 (2006).
66. J. Wang, J. Zhang, and R. Adzic, *J. Phys. Chem. A*, **111**, 12702 (2007).
67. J. Wang, F. Uribe, T. Springer, J. Zhang, and R. Adzic, *Faraday Discuss.*, **140**, 347 (2008).
68. M. Moore, A. Putz, and M. Secanell, *J. Electrochem. Soc.*, **160**, F670 (2013).
69. J. Huang, J. B. Zhang, and M. Eikerling, *Phys. Chem. Chem. Phys.*, **20**, 11776 (2018).
70. B. Jayasankar and K. Karan, *Electrochim. Acta*, **273**, 367 (2018).
71. R. B. Bird, W. E. Stewart, and E. N. Lightfoot, *Transport Phenomena* (John Wiley & Sons, Inc, New York) (2007).
72. A. Kulikovsky, *Electrochem. Commun.*, **4**, 318 (2002).
73. N. Zamel and X. G. Li, *Prog. Energy Combust. Sci.*, **39**, 111 (2013).
74. A. Z. Weber et al., *J. Electrochem. Soc.*, **161**, F1254 (2014).
75. P. Hong, L. F. Xu, J. Q. Li, and M. G. Ouyang, *Energy*, **139**, 277 (2017).
76. M. Sabharwal, L. Pant, A. Putz, D. Susac, J. Jankovic, and M. Secanell, *Fuel Cells*, **16**, 734 (2016).
77. M. Ahadi, M. Tam, M. S. Saha, J. Stumper, and M. Bahrami, *J. Power Sources*, **354**, 207 (2017).
78. O. S. Burheim, H. Su, S. Pasupathi, J. G. Pharoah, and B. G. Pollet, *Int. J. Hydrogen Energy*, **38**, 8437 (2013).
79. O. S. Burheim, H. Su, H. H. Hauge, S. Pasupathi, and B. G. Pollet, *Int. J. Hydrogen Energy*, **39**, 9397 (2014).
80. E. Sadeghi, N. Djilali, and M. Bahrami, *J. Power Sources*, **196**, 246 (2011).
81. C. Fink, S. Gößling, L. Karpenko-Jereb, and P. Urthaler, *Fuel Cells*, **20**, 431 (2020).
82. J. M. LaManna, J. V. Bothe, F. Y. Zhang, and M. M. Mench, *J. Power Sources*, **271**, 180 (2014).
83. S. J. Ridge, R. E. White, Y. Tsou, R. N. Beaver, and G. A. Eisman, *J. Electrochem. Soc.*, **136**, 1902 (1989).
84. J. J. Baschuk and X. H. Li, *J. Power Sources*, **86**, 181 (2000).
85. W. Sun, B. A. Peppley, and K. Karan, *Electrochim. Acta*, **50**, 3359 (2005).
86. A. A. Shah, G. S. Kim, W. Gervais, A. Young, K. Promislow, J. Li, and S. Ye, *J. Power Sources*, **160**, 1251 (2006).
87. D. Gerteisen, T. Heilmann, and C. Ziegler, *J. Power Sources*, **187**, 165 (2009).
88. S. Kamarajugadda and S. Mazumder, *J. Power Sources*, **208**, 328 (2012).
89. N. Khajeh-Hosseini-Dalasm, M. Fesanghary, K. Fushinobu, and K. Okazaki, *Electrochim. Acta*, **60**, 55 (2012).
90. L. Xing, M. Mamlouk, and K. Scott, *Energy*, **61**, 196 (2013).
91. A. Kusoglu and A. Z. Weber, *Chem. Rev.*, **117**, 987 (2017).
92. L. Xing, M. Mamlouk, R. Kumar, and K. Scott, *Int. J. Hydrogen Energy*, **39**, 9087 (2014).
93. D. M. Bernardi and M. W. Verbrugge, *AlChE J.*, **37**, 1151 (1991).
94. T. Suzuki, K. Kudo, and Y. Morimoto, *J. Power Sources*, **222**, 379 (2013).
95. L. Hao, K. Moriyama, W. Gu, and C.-Y. Wang, *J. Electrochem. Soc.*, **162**, F854 (2015).
96. H. Liu, W. K. Epting, and S. Litster, *Langmuir*, **31**, 9853 (2015).
97. J. J. Baschuk and X. Li, *J. Power Sources*, **142**, 134 (2004).
98. P. Berg, A. Novruzi, and K. Promislow, *Chem. Eng. Sci.*, **61**, 4316 (2006).
99. L. X. You and H. T. Liu, *Int. J. Hydrogen Energy*, **26**, 991 (2001).
100. D. T. Song, Q. P. Wang, Z. S. Liu, T. Navessin, M. Eikerling, and S. Holdcroft, *J. Power Sources*, **126**, 104 (2004).
101. K. M. Yin, *J. Appl. Electrochem.*, **37**, 971 (2007).
102. X. X. Zhang, H. Ostadi, K. L. Jiang, and R. Chen, *Electrochim. Acta*, **133**, 475 (2014).
103. D. H. Schwarz and N. Djilali, *J. Electrochem. Soc.*, **154**, B1167 (2007).
104. W. Yoon and A. Z. Weber, *J. Electrochem. Soc.*, **158**, B1007 (2011).
105. F. C. Cetinbas, R. K. Ahluwalia, N. N. Kariuki, and D. J. Myers, *J. Electrochem. Soc.*, **165**, F1051 (2018).
106. K. M. Yin, B. S. Cheng, and K. W. Chiang, *Renewable Energy*, **95**, 191 (2016).
107. L. Xing, Y. Wang, P. K. Das, K. Scott, and W. D. Shi, *Chem. Eng. Sci.*, **192**, 699 (2018).
108. S. Mazumder and J. V. Cole, *J. Electrochem. Soc.*, **150**, A1510 (2003).
109. J. H. Nam and M. Kaviany, *Int. J. Heat Mass Transfer*, **46**, 4595 (2003).
110. C. Siegel, *Energy*, **33**, 1331 (2008).
111. W. Dai, H. J. Wang, X. Z. Yuan, J. J. Martin, D. J. Yang, J. L. Qiao, and J. X. Ma, *Int. J. Hydrogen Energy*, **34**, 9461 (2009).
112. K. Jiao and X. Li, *Prog. Energy Combust. Sci.*, **37**, 221 (2011).
113. X. L. Liu, F. Y. Peng, G. F. Lou, and Z. Wen, *J. Power Sources*, **299**, 85 (2015).
114. W. S. He, J. S. Yi, and T. V. Nguyen, *AlChE J.*, **46**, 2053 (2000).
115. D. Natarajan and T. V. Nguyen, *J. Electrochem. Soc.*, **148**, A1324 (2001).
116. Z. H. Wang, C. Y. Wang, and K. S. Chen, *J. Power Sources*, **94**, 40 (2001).
117. U. Pasaogullari and C. Y. Wang, *J. Electrochem. Soc.*, **152**, A380 (2005).
118. Y. Li and C. Y. Wang, *J. Electrochem. Soc.*, **164**, F171 (2017).
119. E. C. Kumbur, K. V. Sharp, and M. M. Mench, *J. Power Sources*, **168**, 356 (2007).
120. V. Gurau, R. V. Edwards, J. A. Mann, and T. A. Zawodzinski, *Electrochemical and Solid State Letters,*, **11**, B132 (2008).
121. C. Y. Wang, *Electrochemical and Solid State Letters,*, **12**, S2 (2009).
122. U. Pasaogullari and C. Y. Wang, *Electrochim. Acta*, **49**, 4359 (2004).
123. T. Soboleva, K. Malek, Z. Xie, T. Navessin, and S. Holdcroft, *ACS Appl. Mater. Interfaces*, **3**, 1827 (2011).
124. A. Kusoglu, A. Kwong, K. T. Clark, H. P. Gunterman, and A. Z. Weber, *J. Electrochem. Soc.*, **159**, F530 (2012).
125. C. Y. Jung and S. C. Yi, *Electrochem. Commun.*, **35**, 34 (2013).
126. T. Swamy, E. C. Kumbur, and M. M. Mench, *J. Electrochem. Soc.*, **157**, B77 (2010).
127. A. R. Kalidindi, R. Taspinar, S. Litster, and E. C. Kumbur, *Int. J. Hydrogen Energy*, **38**, 9297 (2013).
128. C. Ziegler and D. Gerteisen, *J. Power Sources*, **188**, 184 (2009).
129. H. Wu, X. G. Li, and P. Berg, *Electrochim. Acta*, **54**, 6913 (2009).
130. Y. L. Wang, S. X. Wang, S. C. Liu, H. Li, and K. Zhu, *Electrochim. Acta*, **318**, 770 (2019).
131. B. Andreaus and M. Eikerling, *Device and Materials Modeling in PEM Fuel Cells*, ed. S. J. Paddison and K. S. Promislow (Springer, New York) 41 (2009).
132. M. Eikerling, *J. Electrochem. Soc.*, **153**, E58 (2006).
133. N. P. Siegel, M. W. Ellis, D. J. Nelson, and M. R. von Spakovsky, *J. Power Sources*, **128**, 173 (2004).
134. P. O. Olapade, J. P. Meyers, R. Mukundan, J. R. Davey, and R. L. Borup, *J. Electrochem. Soc.*, **158**, B536 (2011).
135. V. Mulone and K. Karan, *Int. J. Hydrogen Energy*, **38**, 558 (2013).
136. S. Strahl, A. Husar, and A. A. Franco, *Int. J. Hydrogen Energy*, **39**, 9752 (2014).
137. C. Jung, C. Lee, and S. Yi, *J. Membr. Sci.*, **309**, 1 (2008).
138. A. Shah, K. Luo, T. Ralph, and F. Walsh, *Electrochim. Acta*, **56**, 3731 (2011).
139. X.-Z. Yuan and H. Wang, *in PEM Fuel Cell Electrocatalysts and Catalyst Layers: Fundamentals and Applications*, ed. J. Zhang (Springer-Verlag London Ltd, London) 1 (2008).
140. J. Huang, Z. Li, and J. B. Zhang, *Frontiers in Energy*, **11**, 334 (2017).
141. S. A. Li, J. L. Yuan, G. B. Xie, and B. Sundén, *Int. J. Hydrogen Energy*, **43**, 8451 (2018).
142. K. Malek, T. Mashio, and M. Eikerling, *Electrocatalysis*, **2**, 141 (2011).
143. R. M. Darling, *J. Electrochem. Soc.*, **165**, F571 (2018).
144. M. H. Eikerling, K. Malek, and Q. Wang, *in PEM Fuel Cell Electrocatalysts and Catalyst Layers*, ed. J. Zhang (Springer-Verlag London Ltd, London) 381 (2008).
145. D. Harvey, J. G. Pharoah, and K. Karan, *J. Power Sources*, **179**, 209 (2008).
146. X. X. Zhang and Y. Gao, *J. Power Sources*, **318**, 251 (2016).
147. M. Moein-Jahromi and M. J. Kermani, *Int. J. Hydrogen Energy*, **37**, 17954 (2012).
148. A. A. Kulikovsky, *Electrochim. Acta*, **130**, 826 (2014).
149. K. M. Yin, *J. Electrochem. Soc.*, **152**, A583 (2005).
150. P. K. Das, X. G. Li, and Z. S. Liu, *Appl. Energy*, **87**, 2785 (2010).
151. Z. T. Xia, Q. P. Wang, M. Eikerling, and Z. S. Liu, *Canadian Journal of Chemistry-Revue Canadienne De Chimie*, **86**, 657 (2008).
152. G. Lin, W. He, and T. V. Nguyen, *J. Electrochem. Soc.*, **151**, A1999 (2004).
153. P. Jain, L. T. Biegler, and M. S. Jhon, *J. Electrochem. Soc.*, **157**, B1222 (2010).
154. A. A. Kulikovsky, *J. Electrochem. Soc.*, **164**, F379 (2017).
155. K. Broka and P. Ekdunge, *J. Appl. Electrochem.*, **27**, 281 (1997).
156. M. Ismail, D. Ingham, K. J. Hughes, L. Ma, and M. Pourkashanian, *Int. J. Numer. Methods Heat Fluid Flow*, **26**, 1145 (2016).
157. L. Xing, S. F. Du, R. Chen, M. Mamlouk, and K. Scott, *Energy*, **96**, 80 (2016).
158. W.-K. Lee, S. Shimpalee, and J. W. Van Zee, *J. Electrochem. Soc.*, **150**, A341 (2003).
159. A. A. Shah, G. S. Kim, P. C. Sui, and D. Harvey, *J. Power Sources*, **163**, 793 (2007).
160. X. H. Wang and T. V. Nguyen, *J. Electrochem. Soc.*, **155**, B1085 (2008).
161. Q. Ye and T. V. Nguyen, *J. Electrochem. Soc.*, **154**, B1242 (2007).
162. A. Jo, G. Gwak, M. Moazzam, J. Lee, and H. Ju, *Int. J. Hydrogen Energy*, **42**, 3731 (2017).
163. N. P. Subramanian, T. A. Greszler, J. Zhang, W. Gu, and R. Makharia, *J. Electrochem. Soc.*, **159**, B531 (2012).
164. L. M. Pant and A. Z. Weber, *J. Electrochem. Soc.*, **164**, E3102 (2017).
165. I. V. Zenyuk, P. K. Das, and A. Z. Weber, *J. Electrochem. Soc.*, **163**, F691 (2016).
166. A. A. Shah, G. S. Kim, and K. Promislow, *IMA J. Appl. Math.*, **72**, 302 (2007).
167. A. A. Franco, P. Schott, C. Jallut, and B. Maschke, *Fuel Cells*, **7**, 99 (2007).
168. W. K. Epting and S. Litster, *Int. J. Hydrogen Energy*, **37**, 8505 (2012).
169. Y. Ono, T. Mashio, S. Takaichi, A. Ohma, H. Kanesaka, and K. Shinohara, *ECS Trans.*, **28**, 69 (2010).
170. N. Nonoyama, S. Okazaki, A. Z. Weber, Y. Ikogi, and T. Yoshida, *J. Electrochem. Soc.*, **158**, B416 (2011).
171. J. P. Owejan, J. E. Owejan, and W. Gu, *J. Electrochem. Soc.*, **160**, F824 (2013).
172. T. A. Greszler, D. Caulk, and P. Sinha, *J. Electrochem. Soc.*, **159**, F831 (2012).
173. T. Mashio, H. Iden, A. Ohma, and T. Tokumasu, *J. Electroanal. Chem.*, **790**, 27 (2017).
174. V. A. Sethuraman, S. Khan, J. S. Jur, A. T. Haug, and J. W. Weidner, *Electrochim. Acta*, **54**, 6850 (2009).
175. A. Parthasarathy, S. Srinivasan, A. J. Appleby, and C. R. Martin, *J. Electrochem. Soc.*, **139**, 2530 (1992).